Right Ventricle Outflow Tract

7

Farhood Saremi, Siew Yen Ho,
and Damián Sánchez-Quintana

With rapid development in imaging technology, cardiac CT and MR have become the ideal methods for the assessment of complex morphology and function of the conotruncal region including the right ventricle out flow tract (RVOT). Detailed information about the embryology and anatomy of RVOT provides a better understanding of the spectrum of diseases of this region and helps to narrow differential diagnosis of pathologies involving this important structure. This will be discussed first in this chapter. Following to that, the role of CT and MR to evaluate morphology and function in relation to developmental malformation of the RVOT will be reviewed. A spectrum of conotruncal anomalies with abnormally positioned great arteries may arise from a perturbation of RVOT formation. Complications after RVOT surgery in congenital heart disease are common, and many need follow-up imaging for diagnosis and surgical planning. In this regard, the spectrum of diseases, differential diagnosis, and postoperative findings will be described.

F. Saremi, MD (✉)
Department of Radiology, Cardiothoracic Section, University of Southern California, USC Keck Hospital, 1500 San Pablo St., Los Angeles, CA 90033, USA
e-mail: fsaremi@usc.edu

S.Y. Ho, PhD, FRCPath, FESC, FHEA
Cardiac Morphology Unit, Royal Brompton Hospital, London, SW3 6LY, UK

D. Sánchez-Quintana, MD, PhD
Departamento de Anatomía Humana, Facultad de Medicina de Badajoz, Badajoz, 06071, Spain
e-mail: damians@unex.es, dasaqui55@yahoo.com

Developmental Considerations

The two fields of cardiac progenitors are now recognized as the primary, and secondary or anterior, heart fields [1–4]. It is the primary heart field that produces the straight heart tube. In mouse, there is firm evidence that the primary heart field gives rise to the left ventricle (LV), with the secondary field forming both the RV and the outflow tract (OFT) [4]. With looping of the heart tube, the ventricular trabeculations start to form at the outer curvature, permitting identification of the cranial part of the tube as OFT or conotruncus.

The initial OFT extends proximally from the distal ventricular groove to the pericardial reflections and demonstrates a characteristic dogleg bend which divides it into two myocardial subsegments, a proximal subsegment or the conus and a distal subsegment or the truncus [5]. The truncus arteriosus is a short segment interposed between the conus and the aortic sac. The latter transforms into the ascending aorta and pulmonary trunks.

The initial OFT is mainly myocardial and increases almost 6-fold in length between HH12 (Hamburger–Hamilton stages) and 24 (Fig. 7.1) [6]. Subsequently the initial musculature of the walls of the truncus and distal conus disappears by apoptosis, transdifferentiation, absorption into the developing RV, or a combination of

F. Saremi (ed.), *Cardiac CT and MR for Adult Congenital Heart Disease*,
DOI 10.1007/978-1-4614-8875-0_7, © Springer Science+Business Media New York 2014

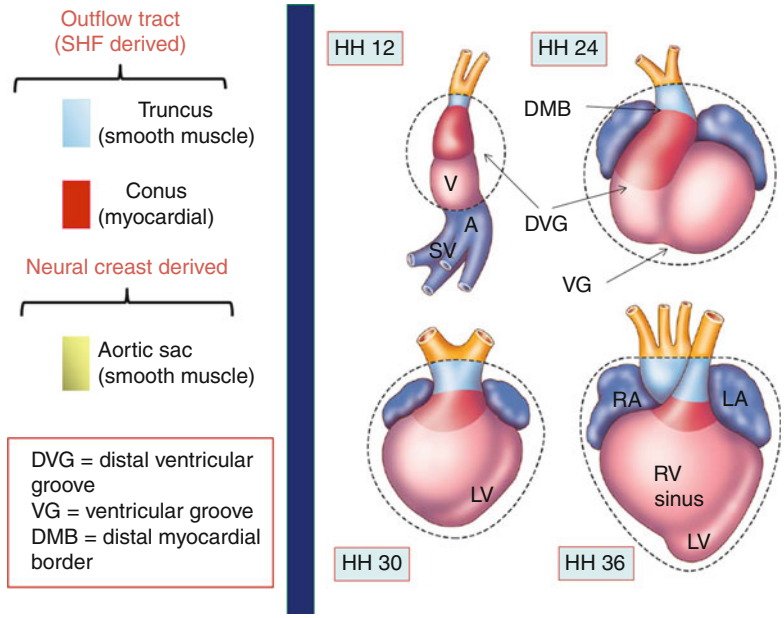

Fig. 7.1 The developing outflow tract in embryonic chicken hearts at stages 12, 24, 30, and 36 H/H. The area of the outflow tract (OFT) extends between distal ventricular groove (*DVG*) of the right ventricle and the junction with aortic sac at pericardial reflections and divided into the conus (proximal OFT shown in red) and the truncus (distal OFT in *light blue*). The OFT is divided into two parts, conus and truncus, and the junction between the two will be distal myocardial border (*DMB*). The images show that the OFT is initially mainly myocardial (*red part*) in its entirety, increasing in length up to HH24. The OFT myocardium, subsequently, shortens as a result of ventricularization, contributing to the trabeculated free wall, as well as the infundibulum, of the right ventricle (*RV*). Note the absolute reduction in the length of the OFT between 30 and 36 H/H stages, as well as the relative reduction in relation to the ventricles, which have increased in size by cardiomyocyte proliferation. The OFT has also been divided by septation into pulmonic and systemic outflows, and the aortic root has rotated to a posterior position, where it connects with the left ventricle (*LV*). The dotted line around the heart indicates the pericardium. *A* primitive atrium, *LA* left atrium, *RA* right atrium, *SV* sinus venosus, *V* primitive ventricle

these processes [7]. With further development, these new portions will be remodeled into the intrapericardial portions of the aorta and pulmonary trunk and arterial valves and their supporting sinuses. In contrast, myocardial tissue is being added to the proximal portion of the conus. As development proceeds, the single OFT undergoes remodeling into separate pulmonary and aortic arteries. The aorticopulmonary septation involves interactions between diverse cell types, including myocardium, endocardium, and neural crest cells [8]. The distal portion of aortic sac is also being considered as an entirely neural crest derivative.

OFT undergoes rotation during its remodeling. Rotation of the myocardium at the base of the OFT is probably essential to achieve normal positioning of the great arteries with respect to each other at the ventriculoarterial junction [9, 10]. In addition to abnormal OFT septation caused by neural crest cell defects, a spectrum of conotruncal anomalies with abnormally positioned great arteries may arise from a perturbation of myocardial rotation including tetralogy of Fallot (TOF), persistent truncus arteriosus, double outlet right ventricle (DORV), and transposition of the great arteries (TGA) [10, 11]. A short outflow tract as obtained experimentally through secondary heart field ablation may not allow a normal conotruncal rotation [4]. Although in conotruncal anomalies including TOF, the infundibular septum is not always short. It is believed that any time the RV shows a short outflow tract, a total or partial lack of conotruncal rotation and remodeling is inevitably present [9] (Fig. 7.2).

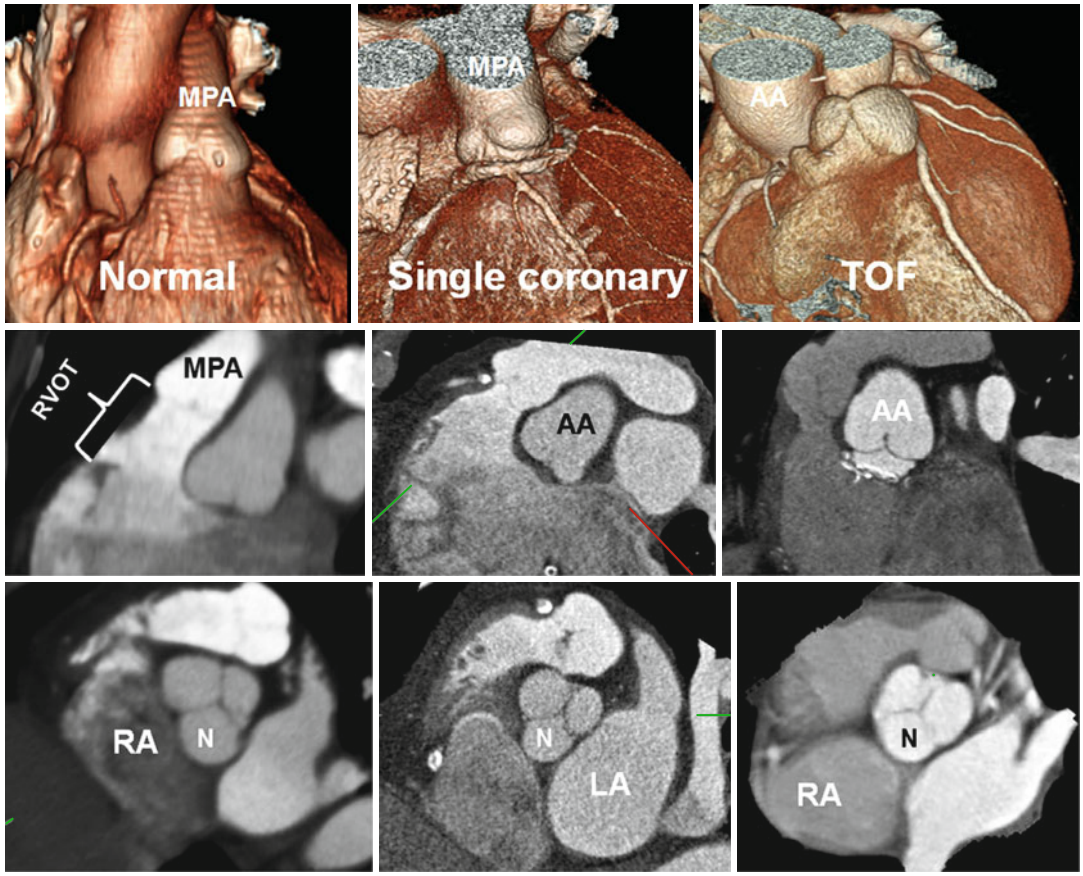

Fig. 7.2 Variations in right ventricle outflow tract (*RVOT*) length. In normal example the pulmonary valve extends well above the coronary sinuses of the ascending aorta (*AA*). The RVOT has a vertical course, and the middle of noncoronary (*N*) sinus overlays the interatrial septum. In patients with single coronary artery arising from the right coronary sinus and tetralogy of Fallot (*TOF*), the RVOT is short, and the aortic root is rotated clockwise facing the right atrium (*RA*). The RVOT is thickened and narrowed in TOF. Although in conotruncal anomalies including TOF the infundibular septum is not always short, it is believed that any time the RV shows a short outflow tract, a total or partial lack of conotruncal rotation is present. *LA* left atrium, *MPA* main pulmonary artery

Anatomical Evaluation of RVOT

Imaging Techniques

Cardiac CT and MR allow comprehensive morphological and functional assessment of the heart within a single examination. Higher spatial resolution and availability of isotropic multiplanar data acquisition of cardiac CT angiography make it the preferred technique over current routine MR techniques for detailed anatomical study of the RVOT. Using new CT scanners, entire heart acquisition can be obtained in a short breath hold combined with thin slices (0.5–0.75 mm). This greatly reduces motion artifacts, and the thin collimation improves the depiction of small structures. Anatomical analysis of the RV can be performed with a dedicated ECG-gated right heart study or as part of CT coronary angiography [12, 13]. In the latter, most of the time sufficient attenuation for visualization of the right heart can be obtained by split-bolus injection in which an initial bolus of contrast medium (50–75 mL) is followed by 50 mL of a 70 %:30 % saline-to-contrast medium mixture and a 30-mL saline chaser at a rate of 4–5 mL/s [13]. A dedicated right heart examination with CT requires ECG gating/triggering and homogeneous enhancement of the

right atrium and ventricle to an optimum Hounsfield unit of 350–400. Scan can be started early (i.e., main pulmonary artery triggering) to include the right heart only. For certain cases with congenital heart disease, a modified injection protocol using dual extremity contrast injections into the antecubital and femoral veins is described which provides homogeneous images of the right atrium and ventricle [14] (Chap. 10 for detail). Different sequences can be used to evaluate the RVOT morphology with MRI including MR angiography, dark/bright blood sequences, and cine images. In addition to routine short- and long-axis cine [ECG-gated cine balanced steady-state free precession (SSFP)] views, transaxial and sagittal images may help to show the abnormality. ECG-triggered, double inversion recovery fast (segmented or single shot) spin-echo sequence with blood suppression is a great technique for anatomical imaging of the outflow tracts and major vessels especially in patients with metallic implant artifacts or those with compromised renal function and contraindication to gadolinium-enhanced MRI.

Anatomical Landmarks

The RV in the normal heart is the most anteriorly situated cardiac chamber and marks the inferior border of the cardiac silhouette. In contrast to the near conical shape of the LV, the RV appears triangular when viewed from the side and crescent shaped when viewed in cross section [15–18]. The curvature of the ventricular septum places the RVOT antero-cephalad to that of the LV's resulting in a characteristic "crossover" relationship between right and left ventricular outflows. This important spatial relationship can be lost in congenital heart malformations such as TGA. The overlap between left ventricular inlets and outlets puts the aortic outflow tract immediately behind the septum that separates it from the RV inlet, giving the "wedged" position of the aortic root.

Traditionally, the RV is divided into the sinus and conus parts, but in more recent decades, both the right and left ventricles have been described as having three components: the inlet, apical trabecular, and outlet portions (Fig. 7.3) [15–17]. In the analysis of congenitally malformed hearts, this tripartite concept is more useful than the traditional bipartite division. The inlet portion of the RV surrounds the leaflets of the tricuspid valve and supports its papillary muscles and tension apparatus. A distinguishing feature of the tricuspid valve is the direct attachment of its septal leaflet to the ventricular septum. The apical portion of the RV is characterized typically by heavy trabeculations. Distinguishing features of the outlet portion of the RV include:

Pulmonary Infundibulum

The pulmonary infundibulum (conus) is a tubular muscular structure that supports the leaflets of the pulmonary valve. Its length, size, and angle vary. The size of the infundibulum is independent of the general size of the RV.

Supraventricular Crest

The posterior (paraseptal) wall of the infundibulum is formed by a prominent muscular ridge, known as the supraventricular crest (crista supraventricularis or ventriculoinfundibular fold) which separates the inlet and outlet components of the RV (Figs. 7.3, 7.4, and 7.5). This is in contrast to the LV where the aortic and mitral valves are in fibrous continuity. Although it looks like a ridge from the perspective of the RV cavity, the supraventricular crest is in fact an infolding of the ventricular wall (the ventriculoinfundibular fold) inserting into the ventricular septum. It is separated from the aorta by the epicardial fat, and any incision through it will lead outside the heart into the vicinity of the right coronary artery (Figs. 7.3 and 7.4). Only the central portion of its inferior most part between the limbs of the septomarginal trabeculation contributes to the interventricular septum (muscular outlet septum or conal septum) [17] (Figs. 7.4 and 7.5). In the normal heart, however, this area is exceedingly small and can hardly be distinguished from the septomarginal trabeculation by CT.

Septomarginal Trabeculation

The septomarginal trabeculation is a prominent Y-shaped muscular strap reinforcing the septal surface. It bifurcates into anterosuperior and

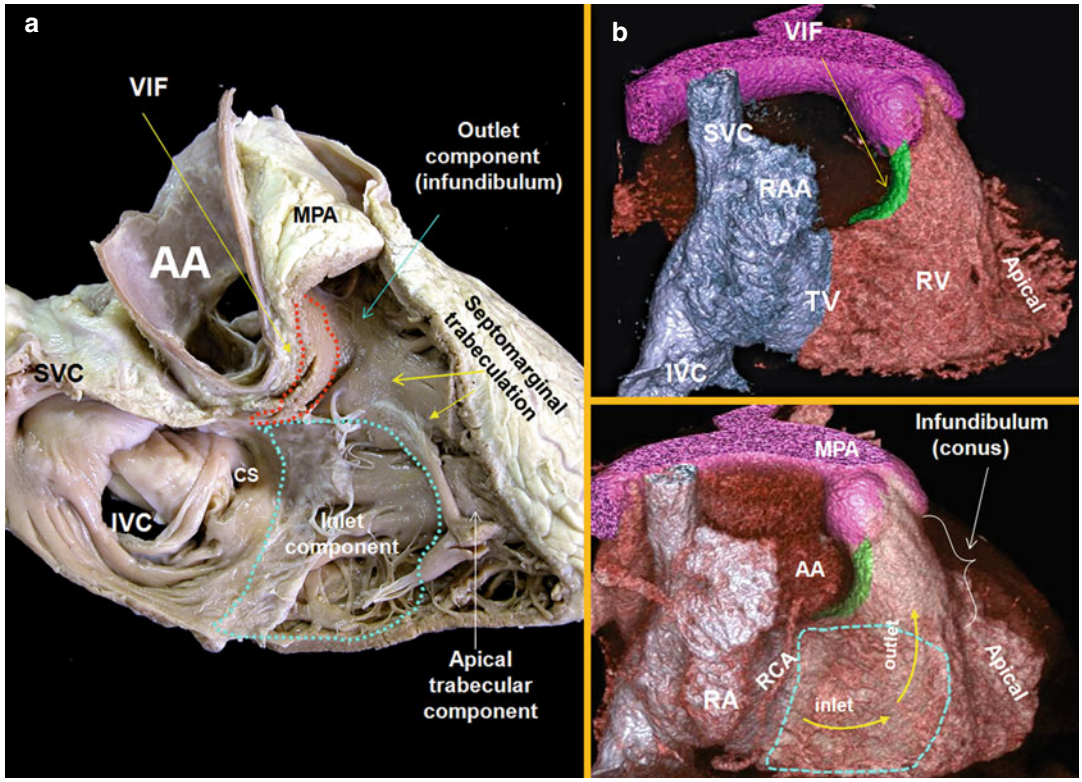

Fig. 7.3 Right anterior oblique views (two chambers) of the right heart are shown. (**a**) Cadaveric specimen. (**b**) Volume-rendered images of a right heart CT. The right ventricle comprises of three components: the inlet, apical trabecular, and outlet portions. The outflow tract, the infundibulum or conus, separates the tricuspid and pulmonary valves. The axis of the orifices of the inlet and outlet roughly forms an angle of 60°. The supraventricular crest is composite of the ventriculoinfundibular fold (*VIF*) cradled between the limbs of septomarginal trabeculation. It is separated from the right aortic sinus by the epicardial fat. *AA* ascending aorta, *MPA* main pulmonary artery, *RA* right atrium, *RAA* right atrial appendage, *SVC* superior vena cava, *IVC* inferior vena cava, *CS* coronary sinus

inferoposterior limbs (Fig. 7.6) which clasp the supraventricular crest. The anterosuperior limb extends along the infundibulum to the leaflets of the pulmonary valve. The posterior limb runs onto and overlays the ventricular septum, toward the right ventricular inlet, giving rise to the medial papillary muscle complex. The body of septomarginal trabeculation extends to the apex of the ventricle, where it gives rise to the moderator band and anterior papillary muscle before breaking up into the general apical trabeculations. The body of the septomarginal trabeculation is interventricular rather than supraventricular and when enlarged can appear as a bump on the septum on cross-sectional imaging. When hypertrophied, the septomarginal band can divide the RV into two chambers (double-chambered RV) [19].

Moderator Band

It is considered as part of the septomarginal trabeculation, supporting the anterior papillary muscle of the tricuspid valve and, from this point, crossing to the free wall of the ventricle. The moderator band incorporates the right atrioventricular bundle, as conduction tissue fibers move toward the apex of the ventricle before entering the anterior papillary muscle. It is usually located equidistant from the tricuspid valve and the apex and can be identified in 90 % of hearts. In 40 % the band is a short and thick trabeculation. The average thickness of the band is 4.5 mm, and its length is 16 mm, ranging from 11 to 24 mm [20]. The moderator band is supplied by branches of the left anterior descending (LAD) artery named the artery of the moderator band. The artery

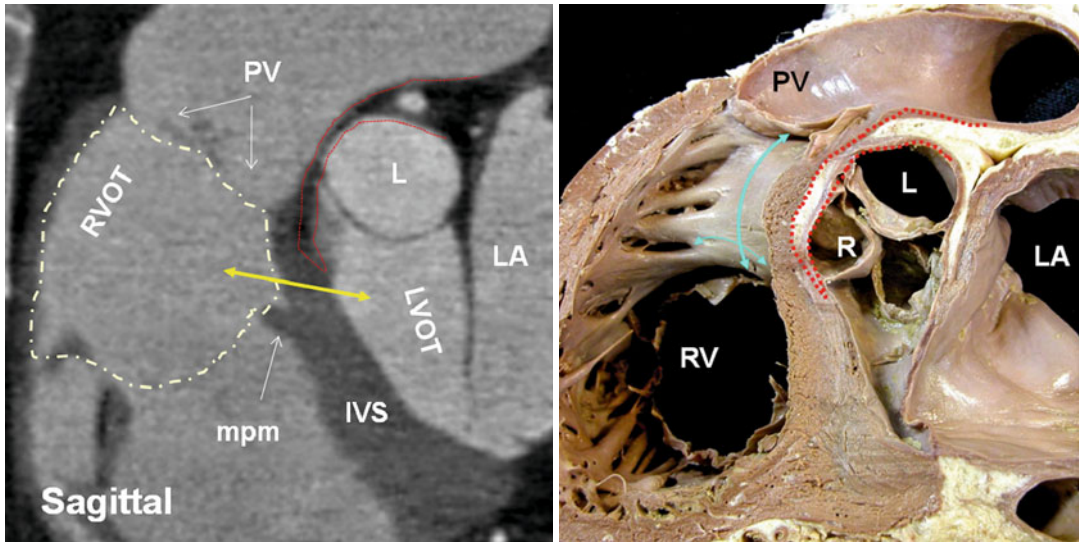

Fig. 7.4 Sagittal views of CT and cadaveric specimen at the right ventricle outflow tract (RVOT). Note fat plane (*dotted red line*) extending between the posterior wall of the RV infundibulum (supraventricular crest) (*blue arrows*) and the anterior wall of ascending aorta making surgical resection of the infundibulum possible. The height of supraventricular crest varies from patient to patient; however, most of it is separated from the aorta by epicardial fat and can be surgically removed without entering the left ventricular cavity. Only the central portion of its inferiormost part may form part of the interventricular septum. The term supraventricular crest is replaced by ventriculoinfundibular fold, representing any muscular structure interposed between the attachments of the leaflets of the atrioventricular and arterial valves. The inferior central part of it is called outlet septum which is part of septomarginal trabeculation. The outlet septum above the level of medial papillary (*double headed yellow arrow*) muscle (mpm) is shown by yellow arrow. However, its true existence is questionable given the limited spatial resolution of CT compared with histological slices. *PV* pulmonary valve, *L* left aortic sinus, *R* right aortic sinus, *RV* right ventricle, *LA* left atrium, *IVS* interventricular septum, *LVOT* left ventricle outflow tract

supplying the band makes anastomotic connections at the base of the anterior papillary muscle with branches of the right coronary artery.

Medial Papillary Muscle of the Conus

The medial (septal) papillary muscle of the conus presents in 82 % of the hearts, while in the rest, it is replaced by tendinous chords [21] (Figs. 7.4 and 7.6). It is a single papilla in 50 % and double in 30 %. It connects with the septal and anterior leaflets of the tricuspid valve. It represents an important surgical landmark for the location of the right bundle branch to avoid injury to the bundle during surgical correction of certain types of ventricular septal defects.

Pulmonary Valve

The pulmonary root is the part of RVOT that supports the leaflets of the pulmonary valve. It consists of three sinuses of Valsalva confined proximally by the semilunar attachments of the valvular leaflets and distally by the sinotubular junction. Different nomenclatures have been used to define the anatomical location of the pulmonary valve sinuses base on their spatial location in relation to the body of the heart itself (Fig. 7.7). Because of the semilunar shape of the pulmonary leaflets (similar to the aortic valve), this valve does not have a ringlike annulus. The sinotubular junction of the pulmonary trunk marks the level of the commissures between the annuli (Fig. 7.7). Compared to the aortic root, the pulmonary sinotubular junction is less obvious on CT images. A second junction exists at the ventriculoarterial junction. The bases of the sinuses within the ventricle cross the anatomical ventriculoarterial junction. The anatomical ventriculoarterial junction forms the annulus. The semilunar attachment of the valvular leaflets which forms the hemodynamic ventriculoarterial

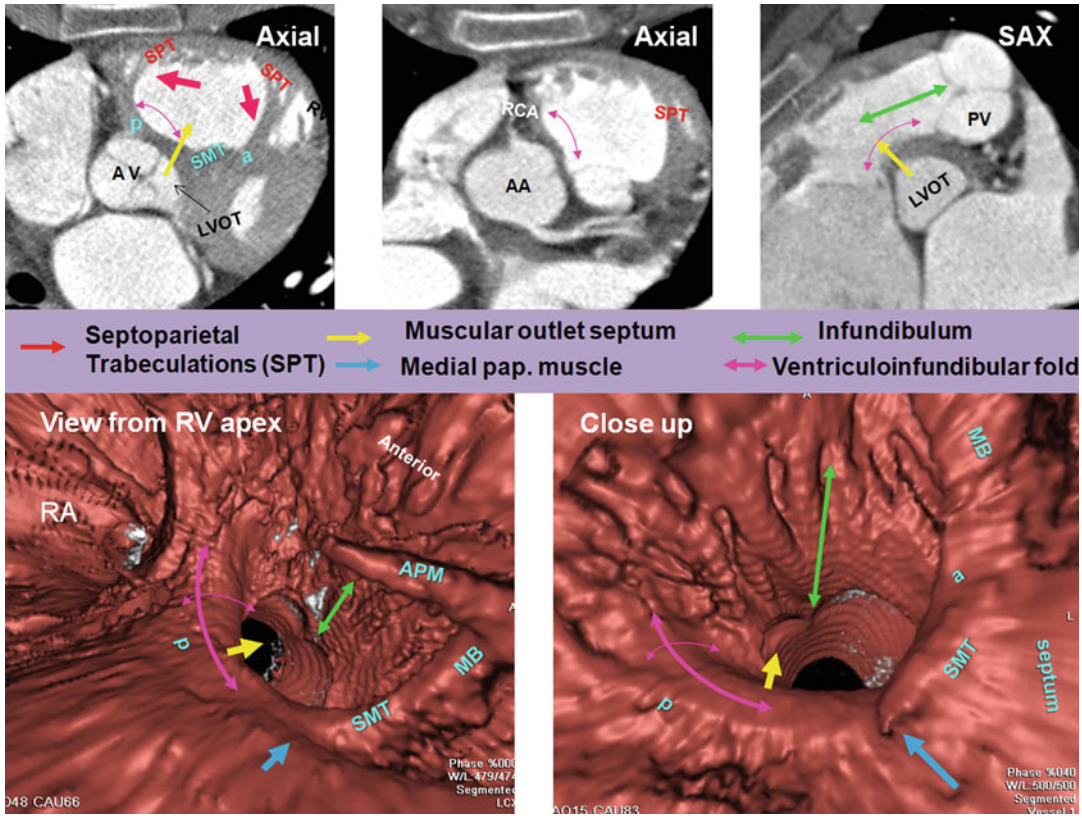

Fig. 7.5 Right ventricle (*RV*) infundibulum. The posterior wall of RV infundibulum is the continuation of the infundibulum into the ventriculoinfundibular fold (supraventricular crest). It is a free-standing wall except its midinferiormost part which contributes to the interventricular septum also known as the outlet septum (*yellow arrows*). One slice above it (second axial cut) at the orifice of the right coronary artery (*RCA*) demonstrates extension of fat plane between the ascending aorta and RVOT. The RCA can be injured at the time of pulmonary valve surgery. The ventriculoinfundibular fold is located between the anterocephalad (septal band) (*a*) and postero-caudal (parietal band) (*p*) limbs of the septomarginal trabeculations (*SMT*), and its width is shown by double-headed purple arrows. The cradle between the SMT limbs and the ventriculoinfundibular fold forms the supraventricular crest. Note smooth surface of ventriculoinfundibular fold compared to the rest of RV infundibulum which is trabeculated. The anterior limb runs superiorly into the infundibulum and supports the leaflets of the pulmonary valve (*PV*). Multiple muscular bundles that extend from the cephalad margin of the septomarginal trabeculation and run onto the parietal wall of the outflow tract are designated as the septoparietal trabeculations (SPT) (*red arrows*). *AA* ascending aorta, *AV* aortic valve, *PUV* pulmonary valve, *MB* moderator band, *RA* right atrium

junction crosses the anatomical ventriculoarterial junction. The leaflets are thickened along their semilunar line of attachment. The fibrous interleaflet trigones are the areas of arterial wall proximal to the semilunar attachments of the leaflets and therefore are incorporated within the ventricular cavity. Their tips point toward the commissures. The musculature of the subpulmonary infundibulum raises the pulmonary valve above the ventricular septum to position the pulmonary valve as the most superiorly situated of the cardiac valves. This anatomical feature makes possible the safe resection of the pulmonary valve, including its basal attachments within the infundibulum from the rest of the RVOT.

Arterial Supply and Anatomical Variants

The conotruncal structures are normally vascularized by anterior and posterior arterial branches

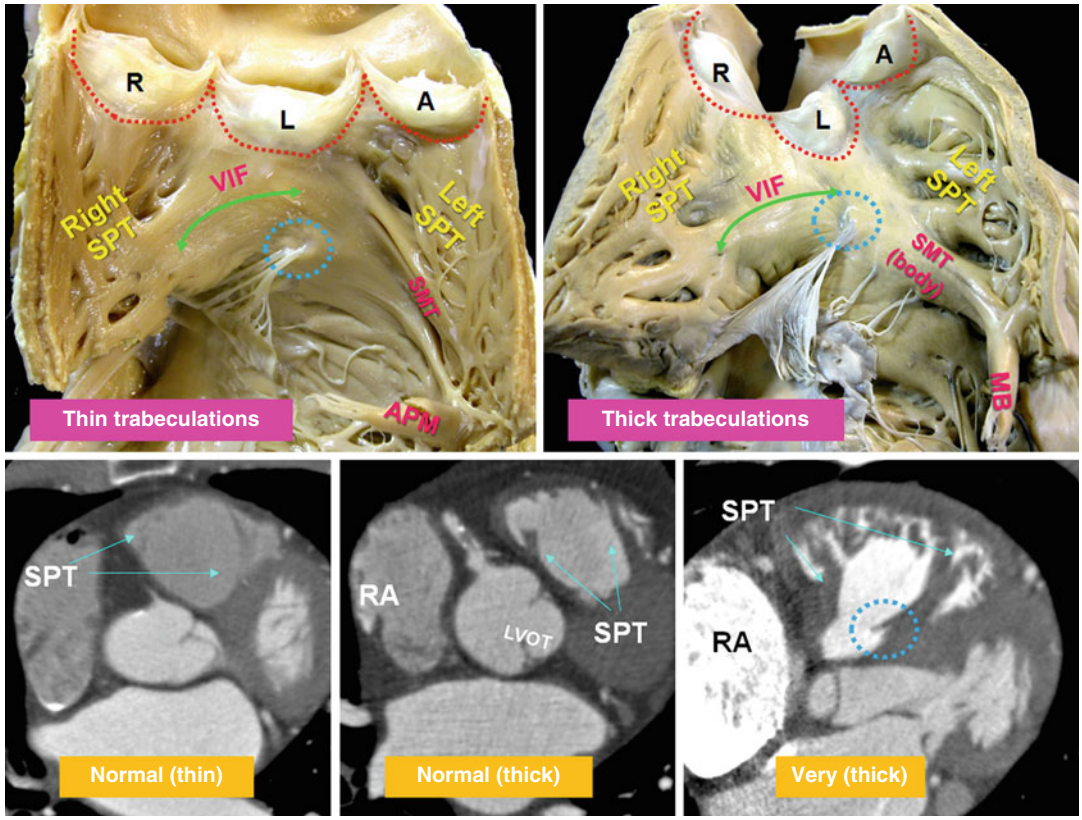

Fig. 7.6 Variation of trabeculations in RVOT. Upper panel: RVOT open-book dissection views. The septomarginal trabeculation (*SMT*) is a muscle strap plastered onto the septal part. The ventriculoinfundibular fold (*VIF*) extends between SMT and the pulmonary valve and forms the paraseptal wall of the RVOT. The septoparietal trabeculations (*SPT*) originate from the anterior margin of the SMT and run round the parietal quadrant of the endocardial infundibulum along the right and left septoparietal walls of the RVOT. These trabeculations vary in number (5–22 trabeculations) and thickness (2–10 mm). The SPTs can be flat or prominent and may be hypertrophied as in pulmonary hypertension or tetralogy of Fallot, contributing to muscular subpulmonary stenosis. The SMT continues to apex and turns into the moderator band (*MB*) and anterior papillary muscle. *Blue circles* demarcate medial papillary muscle. Lower panel demonstrates variable thickness of the SMT and its SPTs. Note marked thickening of the RVOT in the last image in a patient with pulmonary valve stenosis. The right atrium (*RA*) is markedly enlarged. *A* anterior, *R* right posterior, and *L* left posterior are pulmonary sinuses, *LVOT* left ventricle outflow tract, *RA* right atrium, *red dotted line* denotes margin of the pulmonary valve leaflets

from the right and left coronary arteries [22]. On the right side, the branches arise from the conal branch of the right coronary artery or directly from the aorta. On the left side, they arise from the LAD, the left main, or directly from the aorta. The right anterior conal branch is the most constant and conspicuous branch participating in the preconal circulation, also known as Vieussens' arterial ring [22] (Fig. 7.8). This collateral intercoronary connection extends between the conus artery and first right ventricular branch (left anterior conus branch) of the LAD artery. The Vieussens' arterial ring will become dilated when there is proximal LAD artery occlusion or, less frequently, RCA occlusion. Generally, three major collateral pathways at conotruncal level provide circulation between right and left coronary system in all congenital or acquired forms of one-sided coronary occlusion and are used as the basis for different classifications [23]. These three collateral circulation pathways include preconal (precardiac), retroconal (interarterial), and retroaortic. In coronary ostial atresia, because intercoronary collaterals develop very early in

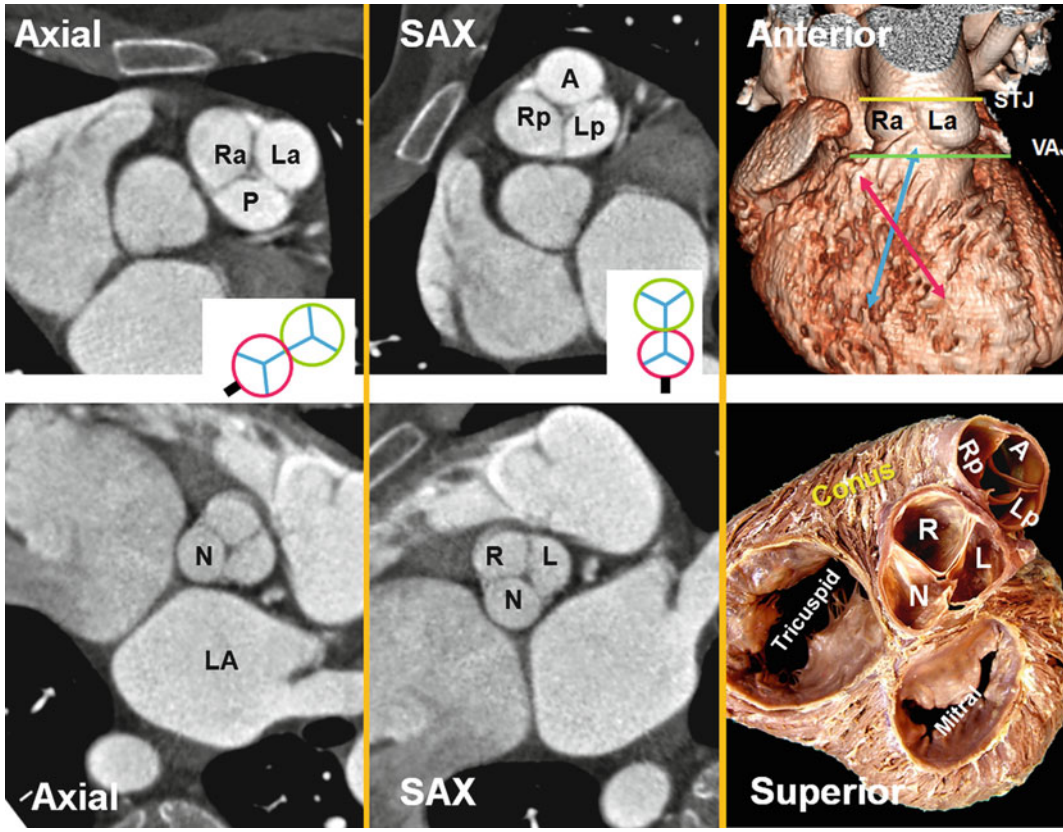

Fig. 7.7 Pulmonary valve sinuses. When heart is viewed in attitudinal anatomical position as sitting in the thorax (i.e., axial views), the pulmonary leaflets and sinuses are seen to be posterior (*P*), right anterolateral (*Ra*), and left anterolateral (*La*). However, in relation to the heart (i.e., short-axis views), the pulmonary sinuses can be named anterior (*A*), left posterior (*Lp*), and right posterior (*Rp*). According to their relation to the aorta, sinuses will be left-facing, right-facing, and nonfacing. Same rule can be applied to the aortic valve as seen in the above examples. The relationship of the pulmonary and aortic valve (*green and red circles*) as well as their orientation in relation to the body (axial) and the heart (short axis, SAX) are drawn; the *black line* shows the location of the interatrial septum. Crossover arrangement between left and right ventricular outflow tracts (*red and blue arrows* respectively) is also shown. The term "pulmonary annulus" denotes the semilunar fibrous attachment of each of the pulmonary leaflets. They are much less sturdy than the aortic annuli. *LA* left atrium, *N* noncoronary sinus, *STJ* sinotubular junction (*yellow line*), *VAJ* ventriculoarterial junction (*green line*)

life, they can be large and overall angiographic appearance of the anomaly can be difficult to differentiate from congenital single coronary artery malformation. In congenital single coronary artery, the blood flow is always centrifugal from larger caliber arteries proximally to smaller ones distally. In ostial atresia the blood flows from the intact right or left coronary artery to the abnormal side via one or more collateral arteries whose caliber is smaller than that of the target vessels (Fig. 7.9). The incidence of a major coronary artery crossing the RVOT in TOF is between 5 and 12 % [24]. Preoperative recognition of such arteries may be important in reconstructive surgery of the RVOT (Fig. 7.10). Infundibular and preventricular branches should not be mistaken for a major coronary artery arising crossing the RVOT.

Morphological Changes in Adult CHD

Major advances in cardiac surgery over the past 50 years have resulted in a marked increase in the number of patients with congenital heart disease

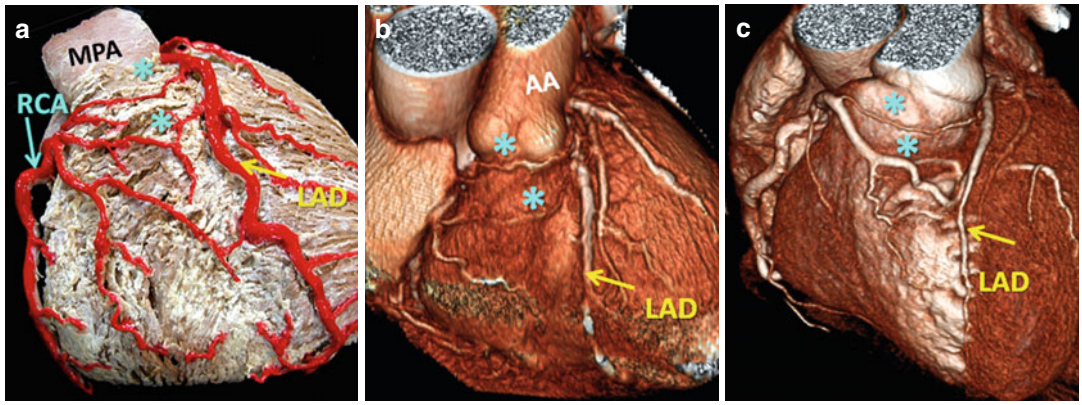

Fig. 7.8 Vieussens' arterial ring; preconal arterial anastomotic rings (*) between pulmonary conus branches arising from the RCA and the LAD artery are shown (**a**) participating in vascular supply to infundibulum as well as the anterior right ventricle. These collaterals may be enlarged in acquired obstructive (**b**) or congenital (**c**) coronary disease. *AA* ascending aorta, *MPA* main pulmonary artery, *RCA* right coronary artery, *LAD* left anterior descending artery

reaching adulthood. In many cases initial surgery is indicated on the basis of echo, with catheterization for physiological assessment if required. CT and MR have a prominent role in follow-up, either to monitor changes during staged surgical repair or to look for complications which are common and many need imaging for diagnosis and surgical planning. However, it is not unusual to discover an RVOT malformation for the first time and without a history of past surgery.

RVOT Stenosis: Pre- and Postoperative Findings

RVOT stenosis is usually secondary to pulmonary valve diseases, but stenotic lesions at subvalvular or supravalvular levels are not uncommon. Causes of RVOT stenosis are listed in Fig. 7.11.

Pulmonary Valve Stenosis

Isolated pulmonary stenosis (PS) is almost always congenital and many can be asymptomatic when first diagnosed. It is not unusual to suspect PS in a young patient on routine chest x-ray or CT by noticing enlarged main and left pulmonary arteries. With severe PS, symptoms of dyspnea, fatigue, chest pain, palpitations, and decreased exercise tolerance may occur. Three morphological types are described [18, 25–28] (Table 7.1). The most common type of congenital PS (40–60 %) is a dome-shaped pulmonary valve, which is characterized by a mobile valve and 2–4 raphes and incomplete separation of valve cusps due to commissural fusion resulting in funnel with a small circular orifice (Fig. 7.12a). The line of basal attachment of the domed valve is not semilunar; instead, the sinuses are shallow and the line attachment appears somewhat circular. A waist-like narrowing of the sinotubular junction may be seen is some cases. Dysplastic pulmonary valve is the second most common PS (20–30 %) and is associated with immobile thickened cusps and in some cases a hypoplastic ventriculoarterial junction [26] (Fig. 7.12b). Cauliflower-like myxomatous thickening is limited to the free margin of the leaflets, and the proximal part of leaflets is intact. The commissures are not fused, the sinuses are deep, and the lines of attachment are semilunar, all as seen in normal hearts. The semilunar attachment of the pulmonary valve leaflets is an essential feature for normal function of the valve. Shallow attachment and lack of "height" of the overall valvular apparatus can cause pulmonary stenosis due to limiting mobility of the free edge of the leaflets even in the absence of commissural fusion. Of those cases with PS who require active treatment whether interventional or surgical, dysplastic

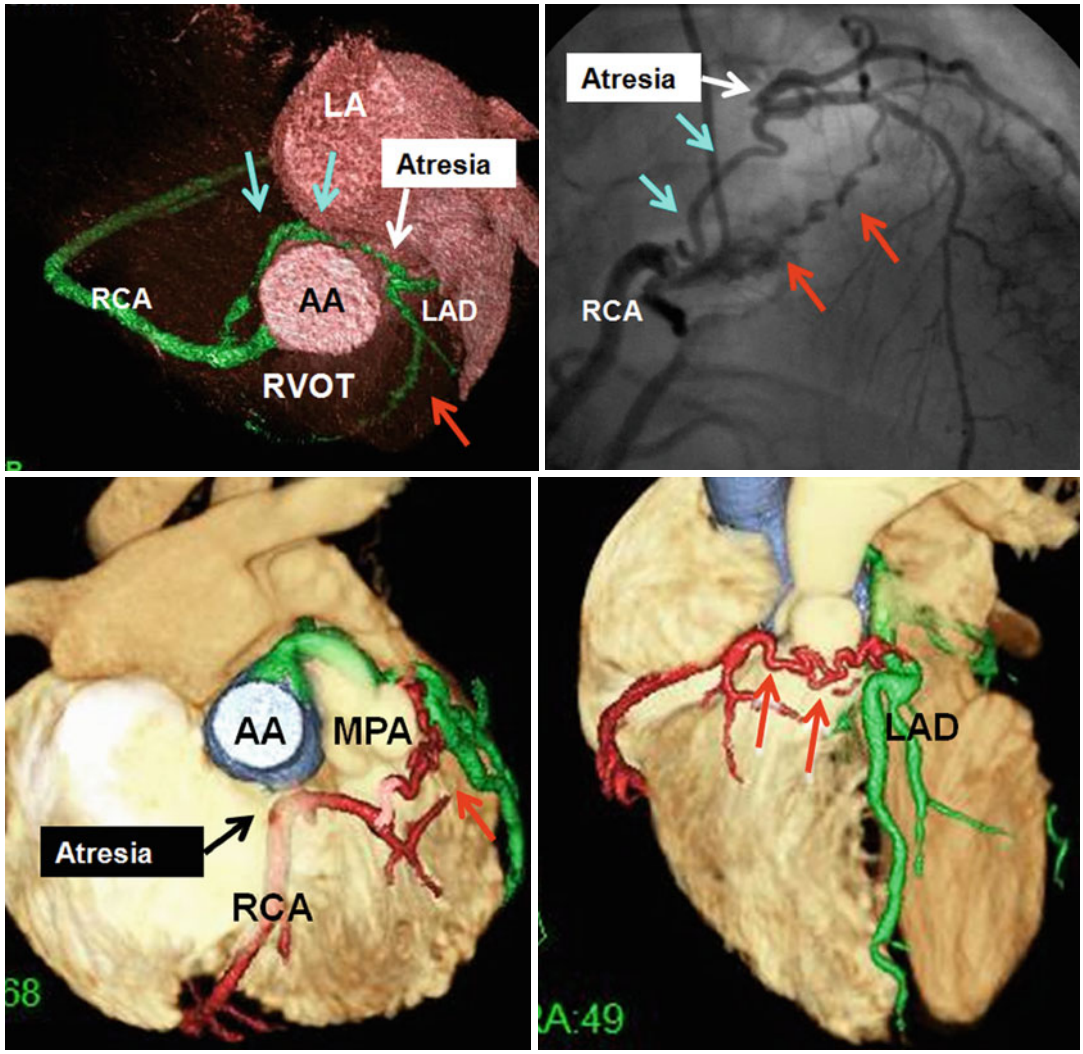

Fig. 7.9 *Upper row* shows left coronary ostial atresia with retroaortic (*blue arrows*) and preconal (*red arrows*) collaterals between the right and left coronary systems. *Lower row* shows right coronary ostial atresia with preconal (*red arrows*) collaterals between the right and left coronary systems in a patient with congenital pulmonary valve stenosis. *AA* ascending aorta, *LA* left atrium, *LAD* left anterior descending artery, *MPA* main pulmonary artery, *RVOT* right ventricle outflow tract, *RCA* right coronary artery

valves would be far more common. Milo et al. [25] described a third morphology of PS with deep "bottle-shaped" sinuses and an hourglass deformity due to supravalvular narrowing at the sinotubular junction (Fig. 7.12c). Although the later morphology is reported in 16 % of patients with congenital PS, it is not accepted as a separate variant by every investigator [26]. Dome-shaped valve with dysplastic leaflets is another uncommon variant. Different morphologies can be equally distinguished with cardiac MR and CT angiography. Bicuspid or multicuspid valve is rare [27] (Fig. 7.13). In bicuspid valve, one leaflet can be larger containing a shallow raphe or both leaflets may be equal in size. Stenosis and post-stenostic dilatation are common. Compared to bicuspid valve, quadricuspid pulmonary valve is usually asymptomatic. Mild pulmonary regurgitation (PR) is not uncommon. Congenital variations can be isolated but are often associated with

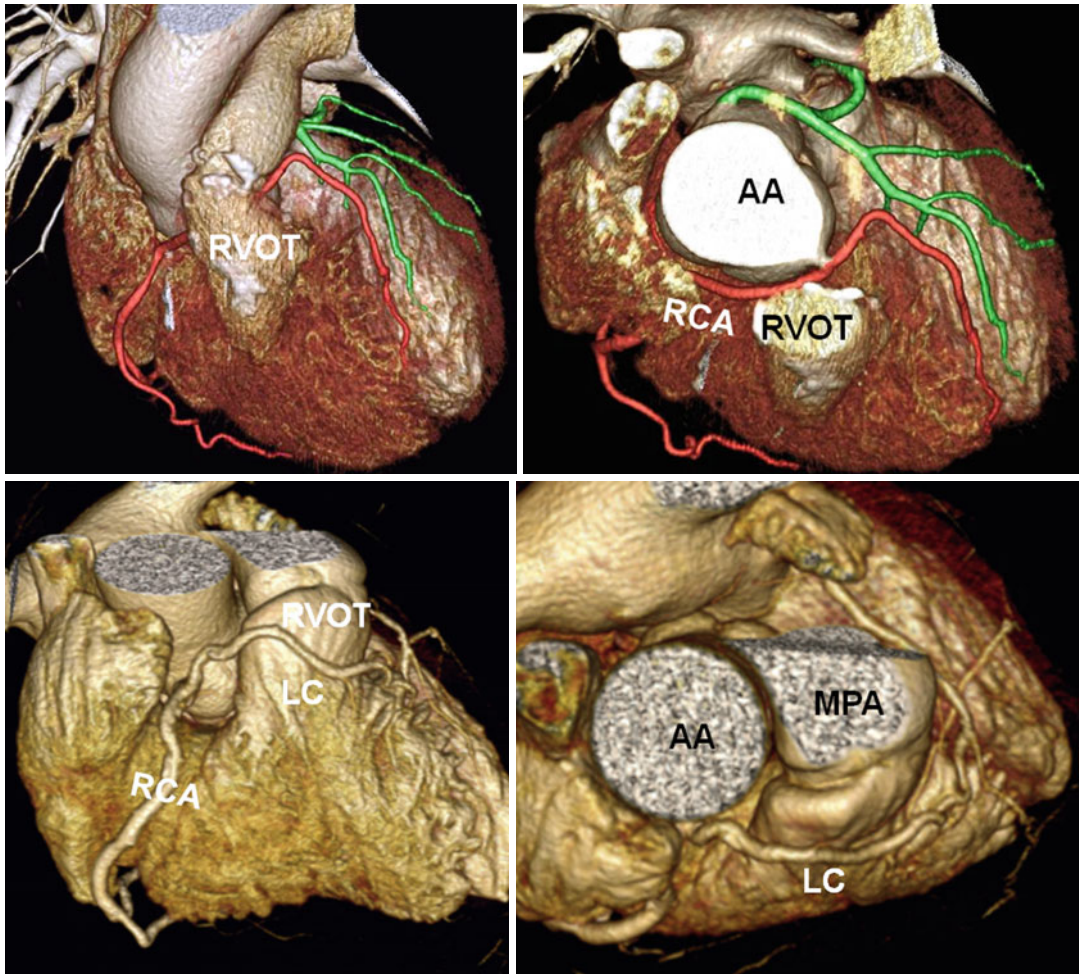

Fig. 7.10 Anomalous course of the coronary arteries next to the right ventricle outflow tract (*RVOT*). *Upper row* shows repaired RVOT in tetralogy. Anomalous course of the right coronary artery (*RCA*) behind the RVOT conduit is seen. *Lower row* shows a single RCA with preconal course of the left coronary (*LC*) artery. *AA* ascending aorta, *MPA* main pulmonary artery

other congenital heart anomalies. For example, tetralogy of Fallot can be associated with a bicuspid pulmonary valve. Congenital pulmonary valve anomalies can also be associated with extracardiac anomalies as in Noonan syndrome and LEOPARD syndrome, which is often associated with a dysplastic pulmonary valve.

Chronic PS results in RV hypertrophy, especially at the RVOT. When prominent, RVOT hypertrophy can lead to secondary dynamic subvalvular stenosis. Distinguishing between valvular stenosis and subvalvular dynamic stenosis secondary to infundibular hypertrophy can become challenging. Subvalvular dynamic obstruction (late systolic stenosis), in fact, often accompanies severe valvular PS and is characterized by a late-peaking jet in MRI similar to that of dynamic LV outflow obstruction. PS can also result in post-stenotic dilatation of the pulmonary trunk and left pulmonary artery. For symptomatic patients with dome-shaped pulmonary valve, balloon valvuloplasty is indicated when a peak instantaneous gradient >50 mmHg is present [28]. A successful procedure is defined by final peak gradient of <30 mmHg and is obtained in >90 % [29]. If the valve is dysplastic, surgery is

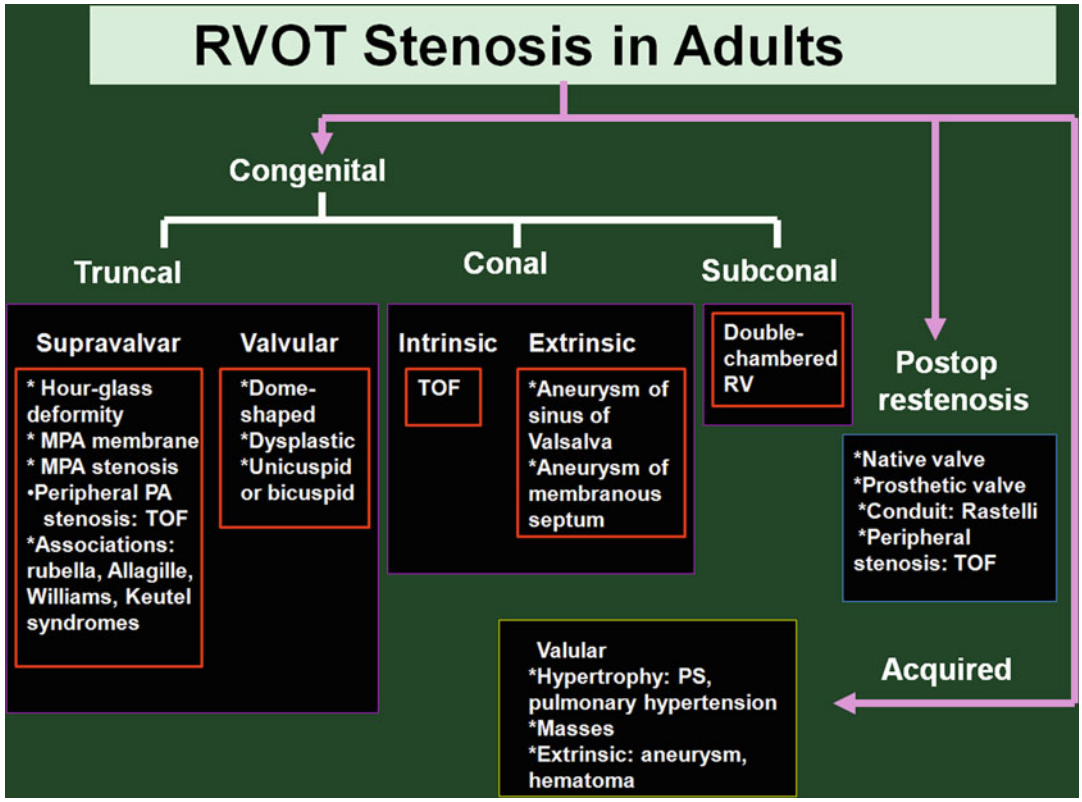

Fig. 7.11 Causes of RVOT stenosis in adults. *TOF* tetralogy of Fallot, *MPA* main pulmonary artery, *PA* pulmonary artery, *PS* pulmonary stenosis, *RV* right ventricle

Table 7.1 Congenital pulmonary valve stenosis

A. Dome-shaped
Very common: 80–90 % of all congenital right ventricle outflow tract lesions
Low familial inheritance
2–4 raphes but no separation into valve cusps
Treatment: balloon valvotomy
B. Dysplastic
10–20 %
Trileaflet with markedly thickened leaflets
Associations: hypoplastic ventriculoarterial junction. Noonan's syndrome
Treatment: partial or total valvotomy, a transannular patch
C. Bicuspid/quadricuspid
Rare
Usually asymptomatic
Common with other congenital heart diseases

more likely to be required; if there is annular or pulmonary trunk hypoplasia, a transannular patch may become necessary. In patients with PS and significant pulmonary regurgitation, valve replacement is required. Mechanical valve replacement is used rarely because of thrombosis issues. Bioprosthetic valves and pulmonary homografts are preferred [30].

Tetralogy of Fallot

TOF consists of a large nonrestrictive subaortic ventricular septal defect (VSD), dextroposed aorta riding up over the septal defect, and RVOT obstruction (Fig. 7.14). TOF without PS is called Eisenmenger complex (Fig. 7.15). Subpulmonary stenosis, which is an essential part of TOF, is mainly due to anterosuperior malalignment of the muscular outlet septum relative to the limbs of the septomarginal trabeculation, coupled with thickened septoparietal trabeculations

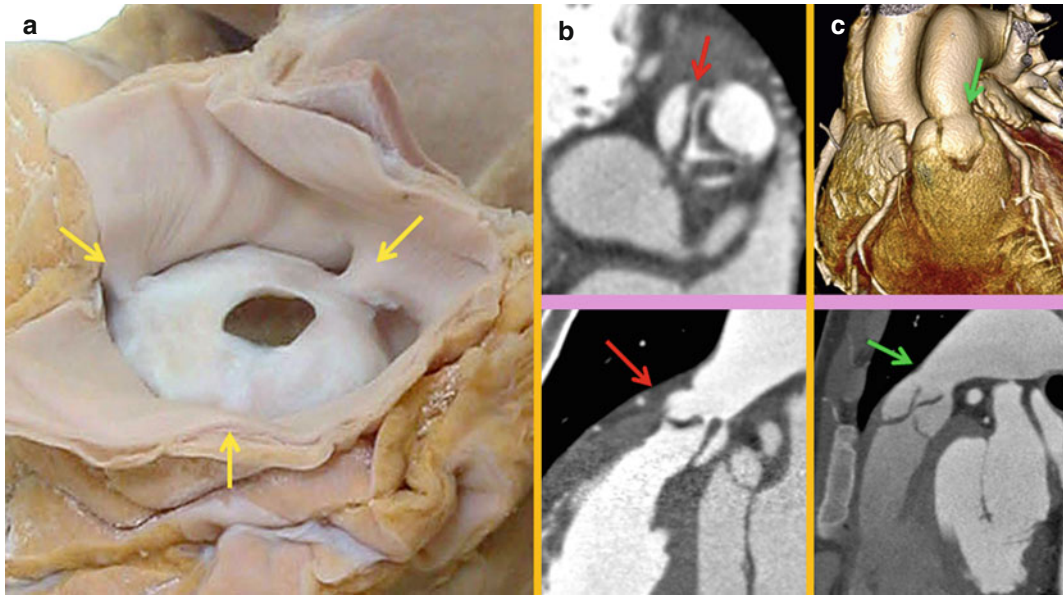

Fig. 7.12 (**a**). Dome-shaped pulmonary valve viewed from the arterial aspect. It is characterized by narrow opening and incomplete separation of the valve cusps. The fused commissures (*yellow arrows*) pull the sinotubular junction toward the central circular orifice. (**b**) Axial and sagittal CT appearance of a dysplastic pulmonary stenosis. Club-shaped myxomatous thickening (*red arrows*) is limited to the free margin of the leaflets, and the proximal part of leaflets appears intact. Note the trileaflet thickened valve and no commissural fusion with hypoplastic ventriculoarterial junction. In dysplastic pulmonary valve, there are three distinct cusps and no commissural fusion. (**c**) Volume-rendered and sagittal CT images in a patient with LEOPARD syndrome and pulmonary stenosis (*arrows*). Note mild thickening of the valve leaflets and narrowing at sinotubular junction giving an hourglass appearance

[17, 31, 32] (Fig. 7.14). Stenosis can also occur at subpulmonic level by hypertrophy of the septomarginal trabeculation or the moderator band. This gives the arrangement often described as "two-chambered right ventricle." The subpulmonary infundibulum itself varies markedly in length and can sometimes be short especially in Eisenmenger complex (Fig. 7.2). In most other instances of TOF, the narrowed infundibular chamber is normal in length but sometimes has considerable length. Absent pulmonary valve syndrome occurs in less than 3–6 % of TOF patients [17]. This syndrome is associated with significant pulmonary artery dilatation and airway compression. Pulmonary atresia in TOF is also due to severe deviation of the outlet septum. However, isolated pulmonary atresia can rarely occur as a result of valve imperforation rather than severe stenosis. In pulmonary atresia blood supply to the right and left pulmonary arteries (if not atretic) will be provided by a large patent ductus arteriosus or multiple aortopulmonary collateral arteries. Extensive reconstructive surgery is required in extreme cases.

Patients with TOF have remarkable intrinsic histological abnormalities and reduced elasticity in both ascending aorta and pulmonary artery, and it appears that TOF repair does not improve these abnormalities [33, 34]. Aortic root dilation with or without aortic regurgitation is common [33]. Cardiac MRI or CT can address these major clinical implications (Fig. 7.14). The concept of aortic overriding is shown in Fig. 7.16. Note that mild overriding above the ventricular septum can be seen in normal instances. Greater than 50 % overriding falls into definition of DORV subgroup. However, in TOF there is always fibrous continuity between the anterior mitral leaflet, while in DORV this may not be the case (Fig. 7.16). The concept of dextroposition is shown in Fig. 7.17.

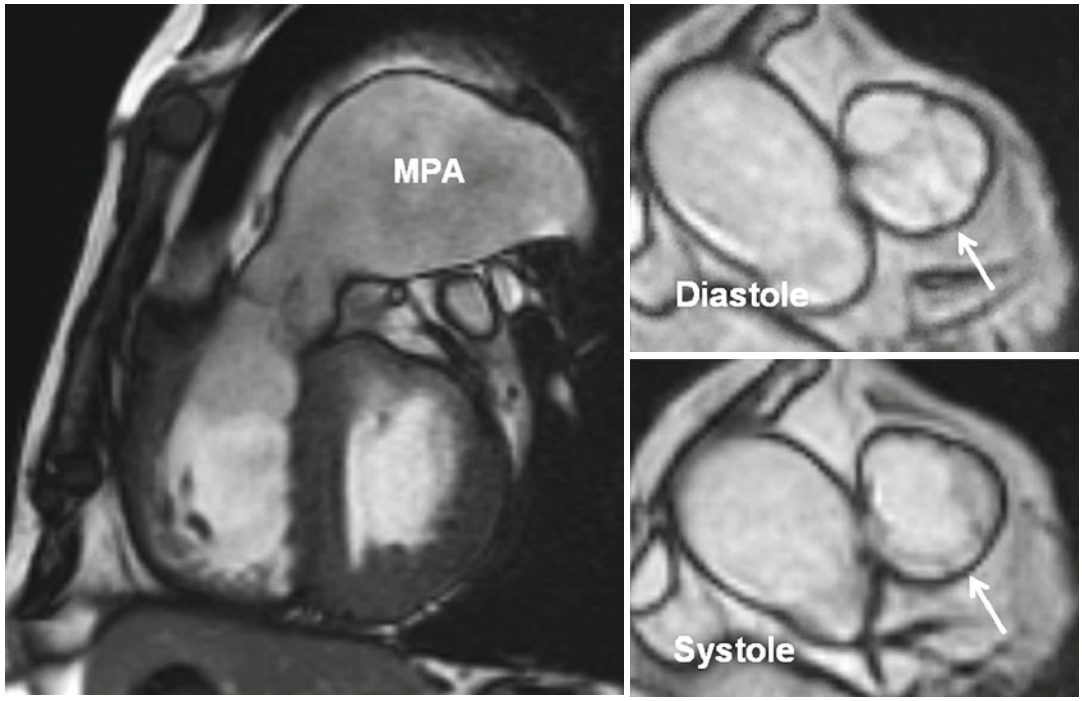

Fig. 7.13 A 51-year-old male with mild pulmonary regurgitation and pulmonary hypertension. Long-axis and short-axis MR images of a quadricuspid valve are shown. The valve is shown at two different phases of cardiac cycle. One rudimentary extra cusp between the left posterior and anterior (nonfacing) cusps (*arrows*) is seen. The right ventricle is hypertrophied and the main pulmonary artery (*MPA*) is dilated

Double-Chambered Right Ventricle

Double-chambered RV (DCRV) is characterized by subinfundibular stenosis due to aberrant hypertrophied septomarginal trabeculations or abnormal moderator band that divides the RV cavity into a proximal high-pressure and a distal low-pressure chamber [19, 35, 36] (Fig. 7.18). The severity of the DCRV stenosis tends to increase with time [36]. DCRV is usually associated with a perimembranous VSD. MRI and CT are usually diagnostic, identifying the degree and location of the obstruction and the presence of a VSD. The degree of stenosis can be best quantified with MR phase-contrast techniques. The indications for surgery in DCRV are similar to those for pulmonary valve stenosis (peak gradients >50 mmHg). Muscular resection and correction of VSD have excellent long-term results and low rates of recurrence [37].

Post-RVOT Repair Changes

Most TOF patients in adult life have undergone either palliative or total repair early in life. Total repair involves a patch closure of the VSD and relief of the RVOT obstruction. In TOF more than one-third of patients receive a transannular RVOT patch using pericardium, Dacron, or polytetrafluoroethylene, and 10 % of TOF patients receive valved conduits, Hancock, homograft, or bovine jugular vein [38]. An extracardiac conduit interposition between the RVOT and main pulmonary artery or individual pulmonary branches may be necessary in the presence of pulmonary atresia or an anomalous left coronary artery crossing the RVOT [39] (Fig. 7.19). Cryopreserved valved aortic homografts are more popular than pulmonary homografts, but accelerated aortic homograft fibrocalcifications have been described [40]. The Contegra valved bovine jugular vein has been used as a better alternative to homografts in

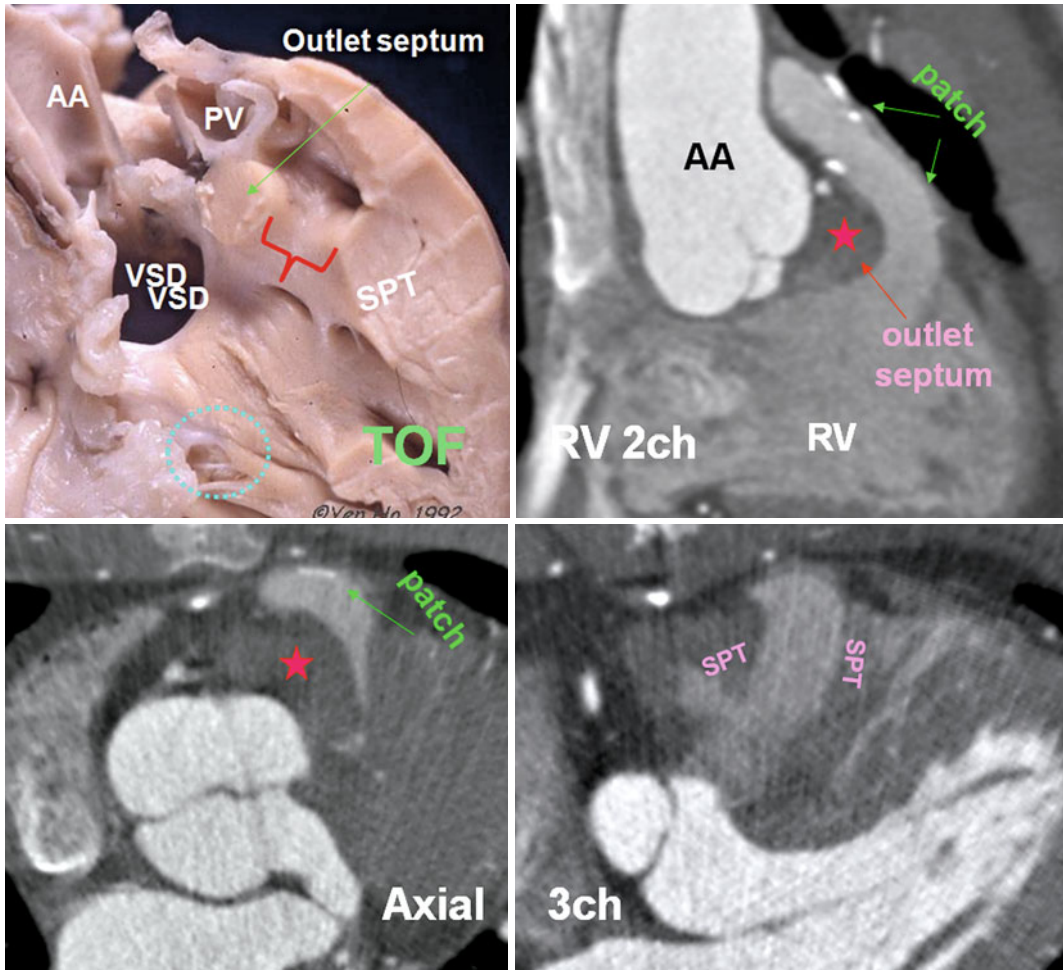

Fig. 7.14 Cadaveric specimen demonstrates phenotypic features of tetralogy of Fallot (*TOF*) including a large nonrestrictive subaortic perimembranous ventricular septal defect (*VSD*) with the aorta overriding the septal defect. The muscular outlet septum is displaced anterocephalad to the limbs of the septomarginal trabeculation, and there is hypertrophy of the septoparietal trabeculations (*SPT*). Subpulmonary obstruction (*red bracket*) is generally produced between the muscular outlet septum and the hypertrophied SPTs. There is continuity between the leaflets of the aortic and tricuspid valves in the postero-inferior margin of the VSD. Note the VSD is located anterior to the medial papillary muscle (*blue circle*). CT images show repaired TOF with markedly thickened outlet septum (*red stars*) and the SPT. Status post transpulmonary patch surgery covering the anterior wall of the RVOT. In this patient the RVOT is long. The ascending aorta (*AA*) is dilated. The muscular outlet septum is located cephalad to the SPTs. *PV* pulmonary valve, *RV 2ch* right ventricle two chamber, *3ch* three chamber

RVOT reconstruction [41]. The diameter of the grafts ranges from 12 to 22 mm and length is 10–12 cm. High pressure in the conduit may lead to aneurysmal dilatation (one-third of the conduits) and valve regurgitation. Dacron conduits are least popular for extensive fibrous sheathing and calcifications (Fig. 7.19). Conduit narrowing at the pulmonary anastomosis (distal suture line) is relatively common which may be associated with conduit dilatation. A complete assessment of pulmonary arterial system with CT or MR may be necessary before RVOT reoperation to find associated complications [42] (Fig. 7.20). Residual branch pulmonary artery stenosis is common after repair. Demonstration of substantial branch pulmonary artery stenosis, especially in the setting of free pulmonary regurgitation, should be treated by balloon dilation with or

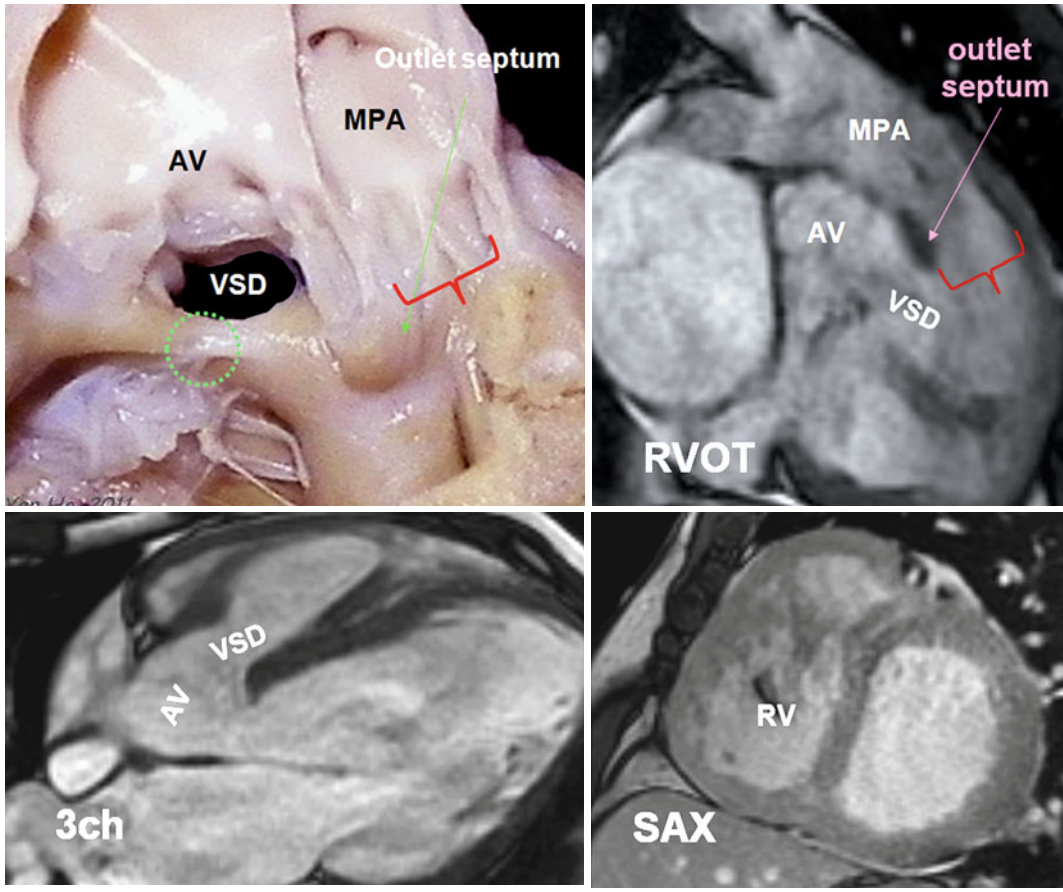

Fig. 7.15 Cadaveric specimen demonstrates phenotypic features of Eisenmenger complex. A subaortic ventricular septal defect (*VSD*) is shown. The outlet septum is mildly displaced superiorly but without causing subpulmonary obstruction (*red bracket*). Note the VSD is located anterior to the medial papillary muscle (*green circle*). MR images are obtained in a 35-year-old male with unrepaired tetralogy. Subaortic VSD and aortic overriding are shown. Outlet septum is superiorly displaced. There is no subpulmonary stenosis (*red bracket*). The right ventricle (*RV*) is thickened wall and appears mildly dilated. *AV* aortic valve, *MPA* main pulmonary artery, *RVOT* right ventricle outflow tract, *SAX* short axis, *3ch* three chamber

without implantation of an endoluminal stent (Fig. 7.21). Repeat sternotomy should be performed with special care in post-OFT surgery cases because of the risk of conduit adherence to the sternum. CT scanning of the chest is helpful in these complex patients (Fig. 7.19).

Recently, percutaneous valve replacement has been performed successfully in RVOT inside a failing bioprosthetic valve or conduit and has now been extended to include patients with native PS [43–45]. Morphology of the RVOT is a major determinant of suitability for percutaneous pulmonary valve replacement. This can easily be done by CT or MRI. Different RVOT morphologies exist (Fig. 7.22). An aneurysmal (pyramidal) [45] morphology is the most common (50 %) and related to the presence of a transannular patch. This morphology is not suitable for percutaneous pulmonary valve implantation. In patients with conduits, other morphologies are more common. The current device for pulmonary valve implantation, made of a platinum–iridium alloy, performs best in cylindrical, rigid (to avoid fracture) RVOTs that measure 14–22 mm diameter. These requirements make the device unsuitable in most of the patients.

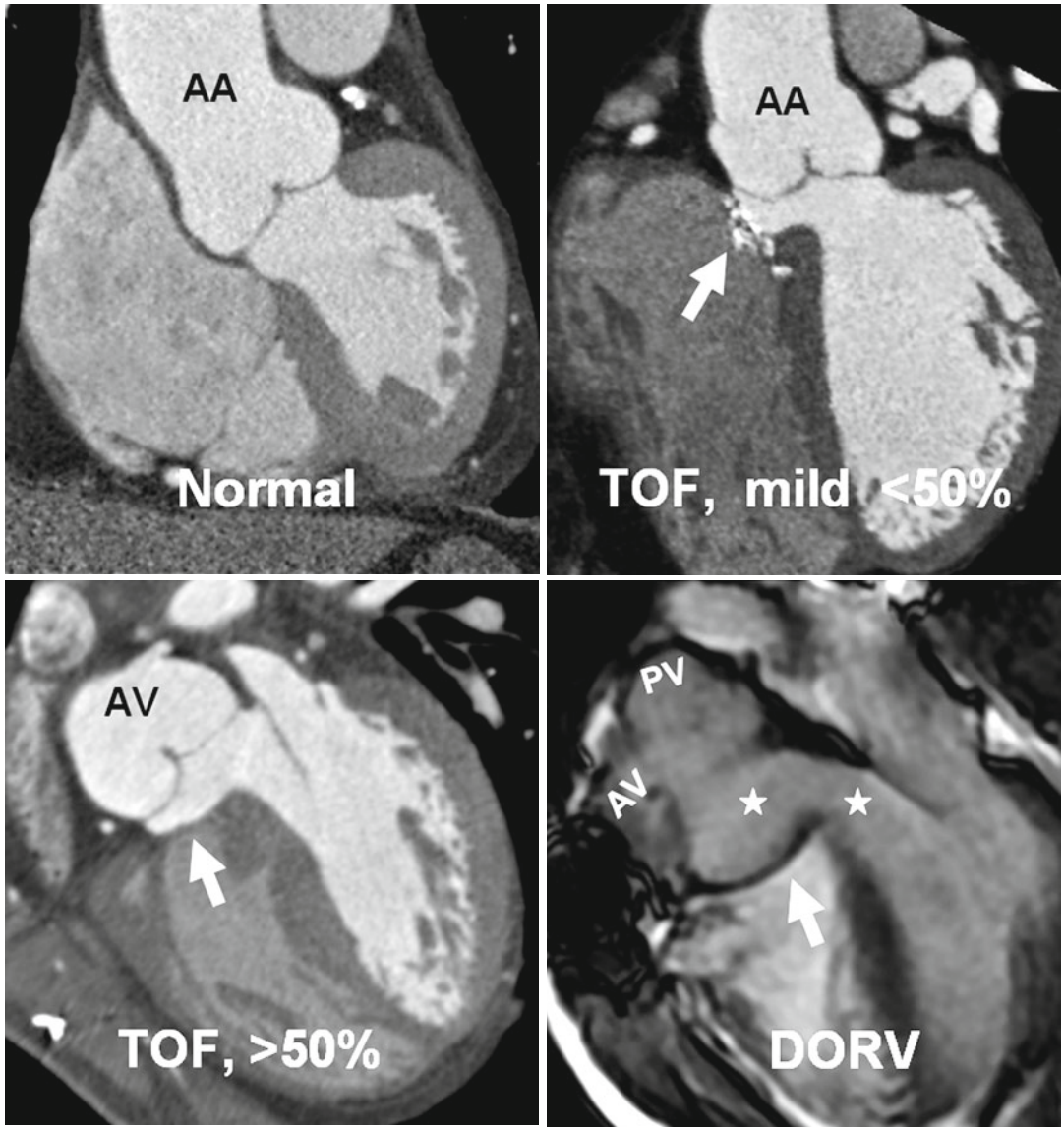

Fig. 7.16 The concept of aortic overriding. Coronal views of the heart at the level of the aortic root demonstrate the relationship of the aorta to interventricular septum. Mild dextroposition of the aorta is normal. When it overrides the septum greater than 50 %, it falls in definition of DORV. However, in this example aortic–mitral fibrous continuity which is essential for diagnosis of TOF still exists. In DORV both aortic valve (*AV*) and pulmonary valve (*PV*) arise from the right ventricle, and the pulmonary valve is usually located on the left side of the aorta. This will result in lack of fibrous continuity between the mitral and aortic valves as shown in this image. *Arrows* point to patch repaired VSDs. *Stars* denote left ventricle baffle. *AA* ascending aorta

Double Outlet Right Ventricle (DORV)

DORV is a type of abnormal ventriculoarterial connection in which both great vessels arise entirely or predominantly (>50 % circumference) from the RV [46]. New classification defines four types of DORV based on the clinical presentation and surgical treatment approach: VSD type (24 %), Fallot type (36 %), TGA type (Taussig–Bing) (18 %), and DORV noncommitted VSD (22 %) [47–49]. The VSD is typically large and has four potential locations: subaortic, subpulmonic, doubly committed, or remote

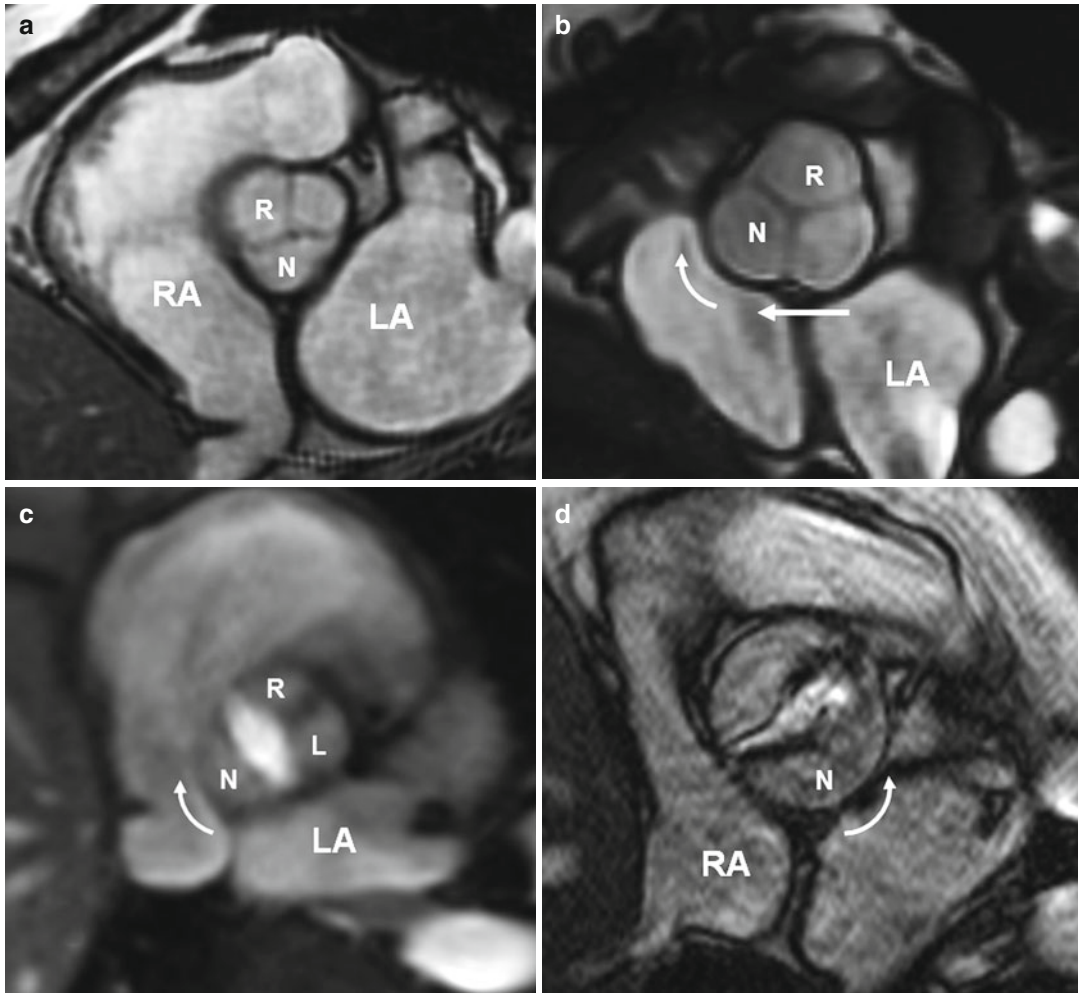

Fig. 7.17 The concept of dextroposition. The term dextroposition indicates that there is specific anatomical evidence that the aortic root is rotated in a clockwise direction (looking from below) and is partially transposed to the right. (**a**) Normal heart with normal aortic root showing the noncoronary aortic sinus (*N*) facing the interatrial septum. In normal patients mild clockwise rotation of the aortic root toward the right atrium (*RA*) is not unusual. (**b**) Typical changes of the aortic root in tetralogy of Fallot (TOF) including clockwise rotation (*curved arrow*) and rightward translation (*straight arrow*). The root is also dilated causing aortic regurgitation in many adult TOF cases. Aortic root rotation is not limited to TOF and is seen in many conotruncal anomalies. (**c**, **d**) Demonstrate changes of the aortic root in two patients with bicuspid aortic valve, one with a raphe between the right (*R*) and the left (*L*) sinuses (**c**) and second without the raphe (**d**). Clockwise rotation is seen in **c** and counterclockwise rotation in (d). (**d**) Shows aortic stenosis. *LA* left atrium

noncommitted [47]. MR is accurate in pre- and postoperative assessment of DORV patients [50]. The spatial relationship between semilunar valves, great arteries, outlet septum, and VSD can be accurately assessed by MRI [50, 51]. The data for the role of CT in DORV is limited. In one study using electron beam CT, the range of diagnostic accuracy for all VSD types in DORV was 88–100 % for 3D CT and 71–94 % for echocardiography [52]. CT also provides clear delineation of the outlet septum which defines the location of the VSD. The outlet septum attaches to the anterior or posterior limbs of septomarginal trabeculations in subaortic or subpulmonic VSDs respectively. In the doubly committed VSD, the muscular outlet septum is

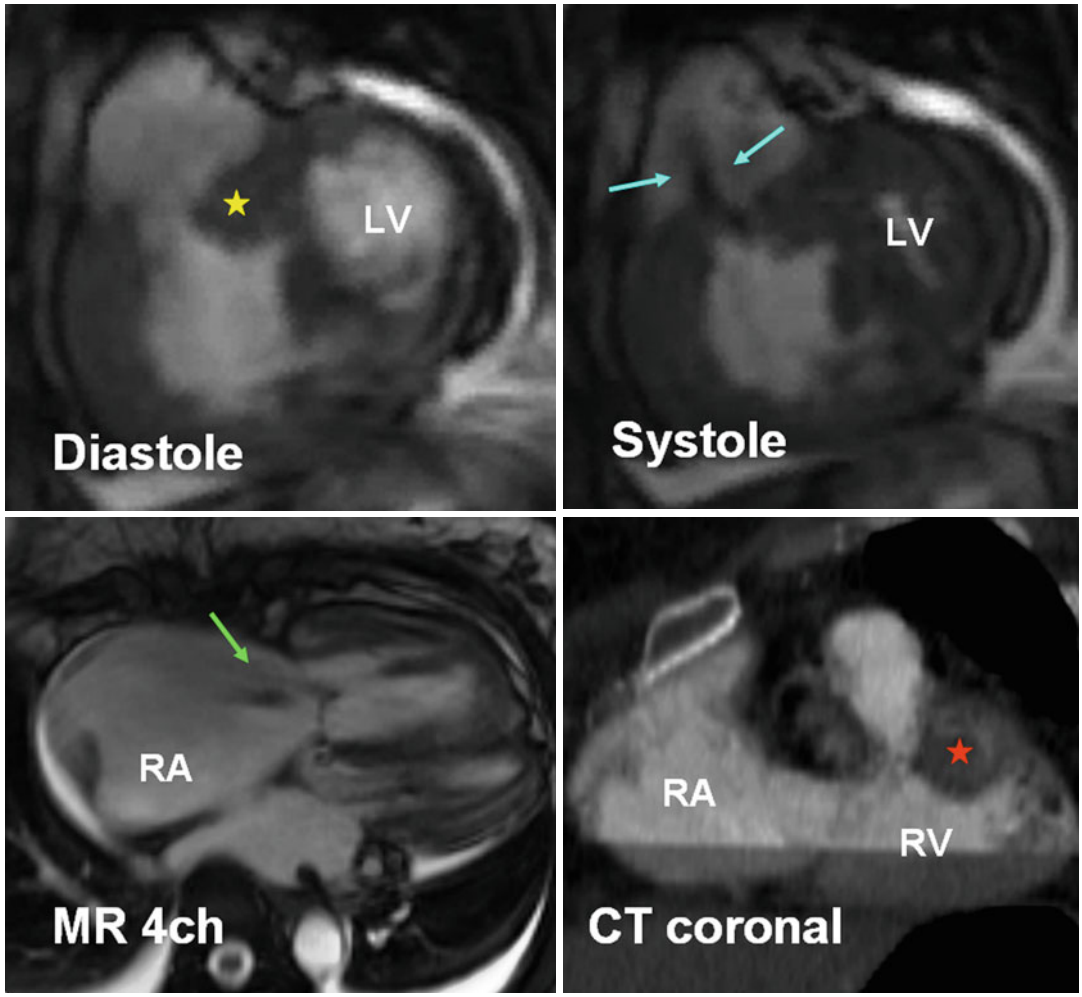

Fig. 7.18 A 48-year-old female with double-chambered right ventricle (*RV*). Severe RVOT stenosis is seen as a result of thickened septomarginal (*yellow star*) and septoparietal (*red star*) trabeculations. Jet flow is seen in systole (*blue arrows*). Thickened wall RV inlet is shown. The right atrium (*RA*) and the RV are enlarged, and there is mild to moderate tricuspid regurgitation (*green arrow*). *LV* left ventricle

absent [48]. The arterial trunks may vary in location, with the aorta generally to the right of the pulmonary trunk (Fig. 7.23). If the trunks spiral as they leave the base of the heart, the VSD is usually subaortic. If the trunks are parallel with the aorta anterior and rightward, the VSD is usually subpulmonic. When the VSD is only under the pulmonary trunk, the configuration is called the Taussig–Bing heart [18, 48]. Usually, there is no fibrous continuity between the semilunar and atrioventricular valves with both great arteries arising predominantly from the RV.

Postoperative DORV

Depending on the anomaly, different surgical methods are used in DORV. In unrestrictive subaortic VSD type, the VSD is closed to include the aortic valve as part of the LV, creating a tunnel that excludes the RV from the systemic circulation. An intraventricular tunnel made of a Gore-Tex patch can baffle blood from the LV through the VSD to the aorta [53, 54]. In Fallot type there is usually a subaortic VSD with pulmonary stenosis. A Rastelli repair is performed, with creation of an intraventricular tunnel to baffle LV to the aorta and placement

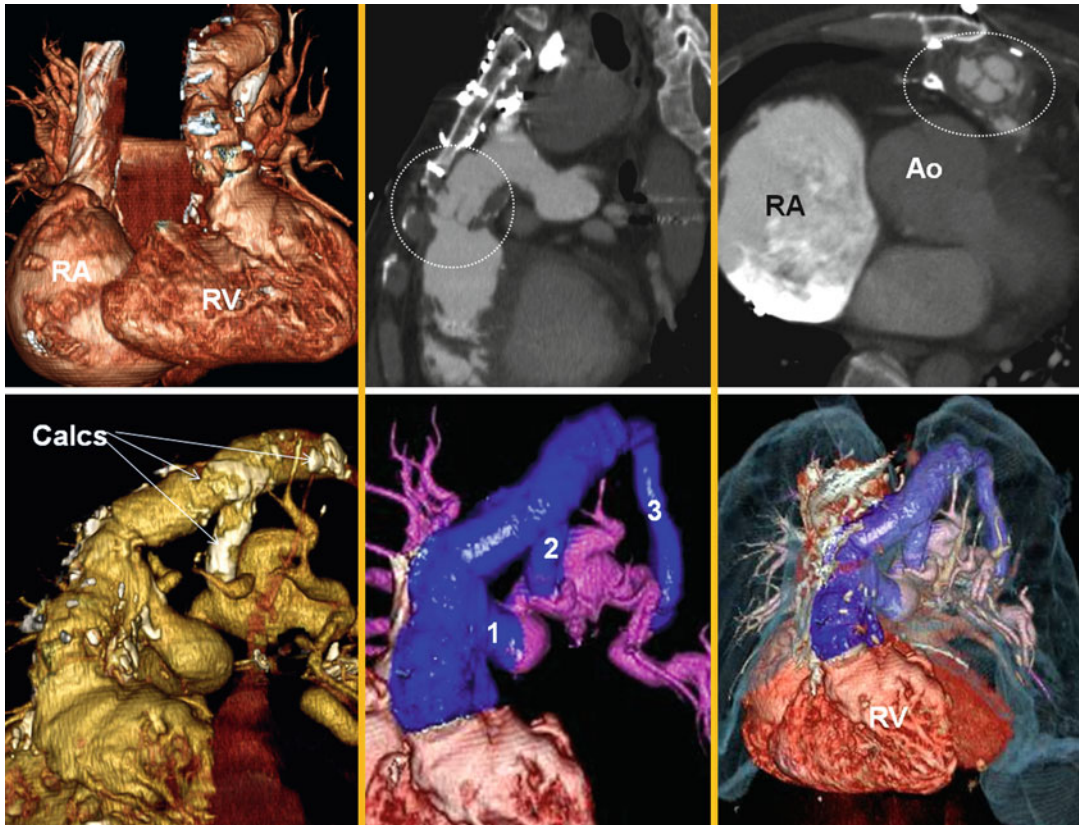

Fig. 7.19 A 48-year-old with history of tetralogy of Fallot (TOF) and pulmonary atresia. Long conduit is shown (*blue colored*) extending between the right ventricle outflow tract and left pulmonary artery branched with three separate connections (*1–3*) to the left pulmonary artery branches. The right atrium (*RA*) and right ventricle (*RV*) are markedly dilated. The aorta is also enlarged (*Ao*). Note close approximation of the pulmonary valve conduit to the sternum (*white circles*). Extensive calcifications (calcs) are shown

of a RV-to-pulmonary artery conduit (valved homograft) (Fig. 7.23). TGA type usually has a subpulmonary VSD without pulmonary stenosis. Complete repair with an arterial switch operation and a VSD to pulmonary artery baffle is required in the neonatal period. Repair of DORV with a remote noncommitted VSD can be very complex [53]. In postoperative cases MRI or CT can easily shows the morphology and patency of both outflow tracts. In postoperative patient, issues that should be assessed with imaging include the status of both ventricles, any evidence for subaortic or subpulmonary obstruction if a tunnel-type operation has been performed, the presence of a residual VSD, and evidence for conduit stenosis or regurgitation.

Complete Transposition of the Great Arteries

In this anomaly ventriculoarterial discordance exists, meaning the aorta arises from the morphological RV and the pulmonary artery arises from the morphological LV [55, 56] (Fig. 7.24a, b). In TGA the aorta and main pulmonary artery are parallel rather than crossing, and in most cases the aorta is located right anterior to the pulmonary artery (Fig. 7.24). It is not uncommon to see the aorta directly anterior to the pulmonary artery [57]. Rarely, the arrangement is side-by-side, with the aorta on the right and in front of the tricuspid valve [58]. RV dysfunction and pulmonary hypertension are recognized late outcome after the Mustard or Senning procedures [59, 60]. In arterial switch

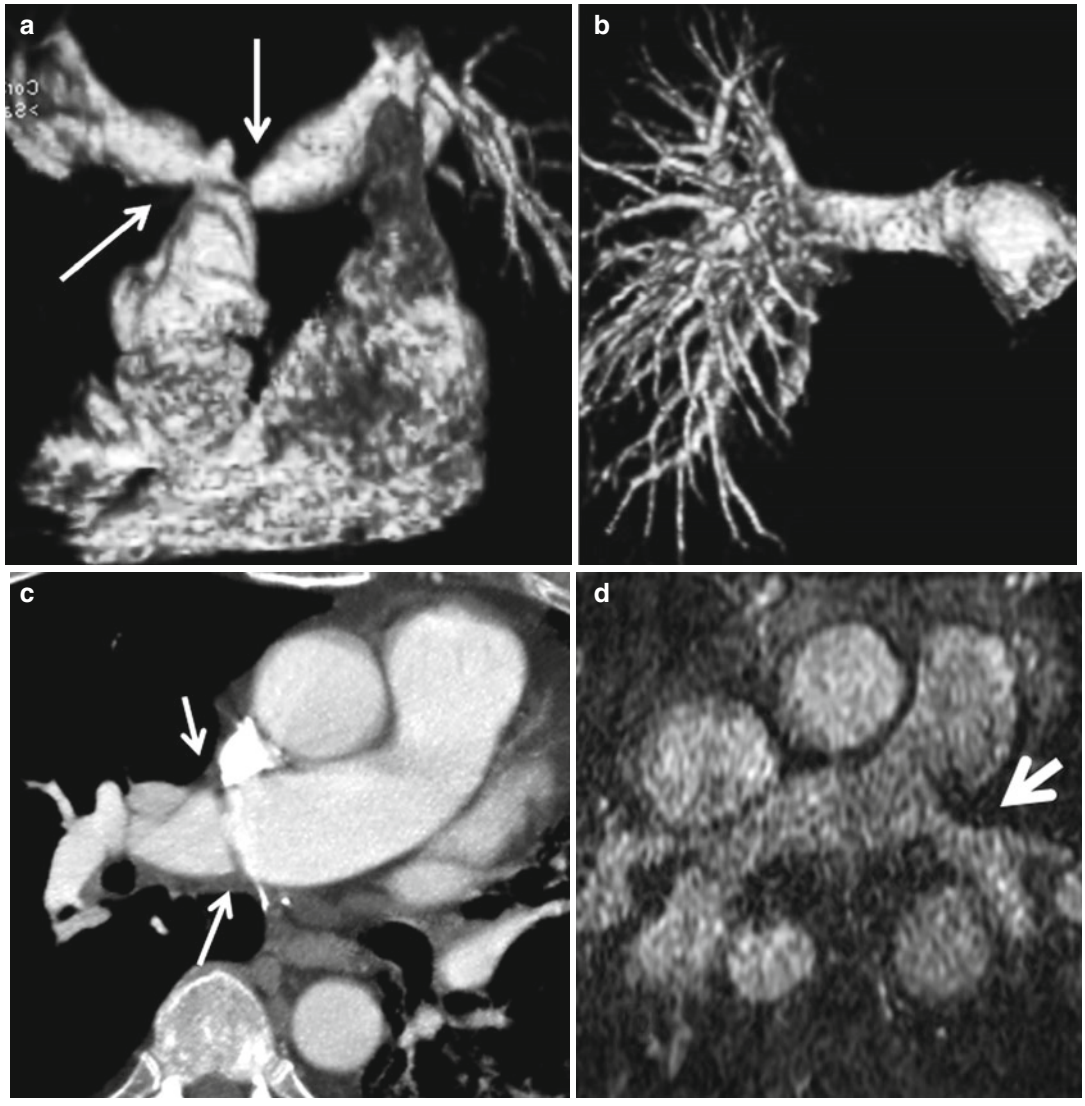

Fig. 7.20 Associated findings in pulmonary branches of different adult patients with repaired TOF represented with RVOT regurgitation. A comprehensive assessment of pulmonary branches is necessary before pulmonary valve implantations. (**a**) Severe right and left pulmonary arteries stenosis (*arrows*). (**b**) Absence of left pulmonary artery. (**c**) Annular stenosis of distal right pulmonary artery (*arrows*). (**d**) Mild narrowing of left pulmonary artery (*arrow*)

Fig. 7.22 Morphology of the RVOT in repaired TOF is a major determinant of suitability for percutaneous pulmonary valve replacement. Untreated TOF is shown for comparison (female 54 years old). Type I is aneurysmal (pyramidal) shape and the most common (50 %) and not a good candidate for valve replacement. Type II is cylindric with a constant diameter (14 %). Type III has an inverted pyramidal appearance (3 %), Type IV is fusiform (17 %), and Type V is narrow and tubular (13 %). Note stenosis at distal end of homograft in the fusiform RVOT. MR or CT is necessary for 3-dimensional analysis and appropriate measurements. MR assessment of right and left pulmonary arteries is necessary for hemodynamic analysis in each candidate

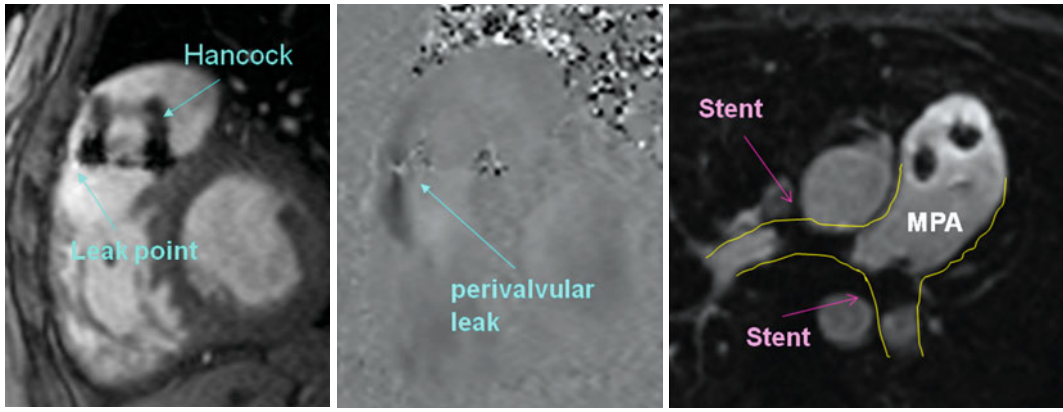

Fig. 7.21 Tetralogy of Fallot (TOF) with anterior perivalvular leak (*blue arrows*). Status post Hancock pulmonary valve replacement and stenting of right and left pulmonary arteries (*pink arrows*). The metallic struts of the bioprosthetic valve cause artifacts that compromised a full evaluation of the pulmonary valve. The measured regurgitant fraction from the perivalvular insufficiency was approximately 15 %. The proximal portion of the main pulmonary artery (*MPA*) was aneurysmal measuring 4.8×3.8 cm. Substantial branch pulmonary artery stenosis was treated by balloon dilation and endoluminal stent before valve replacement

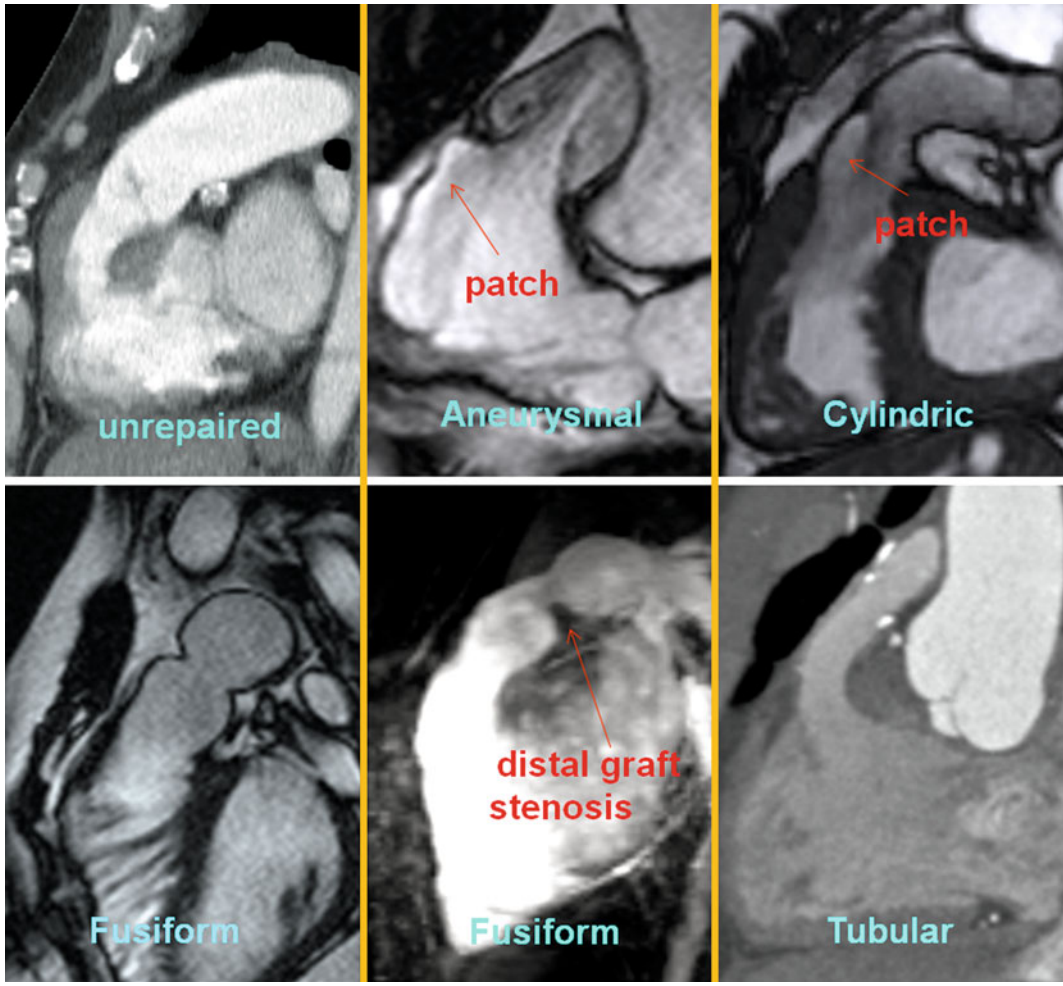

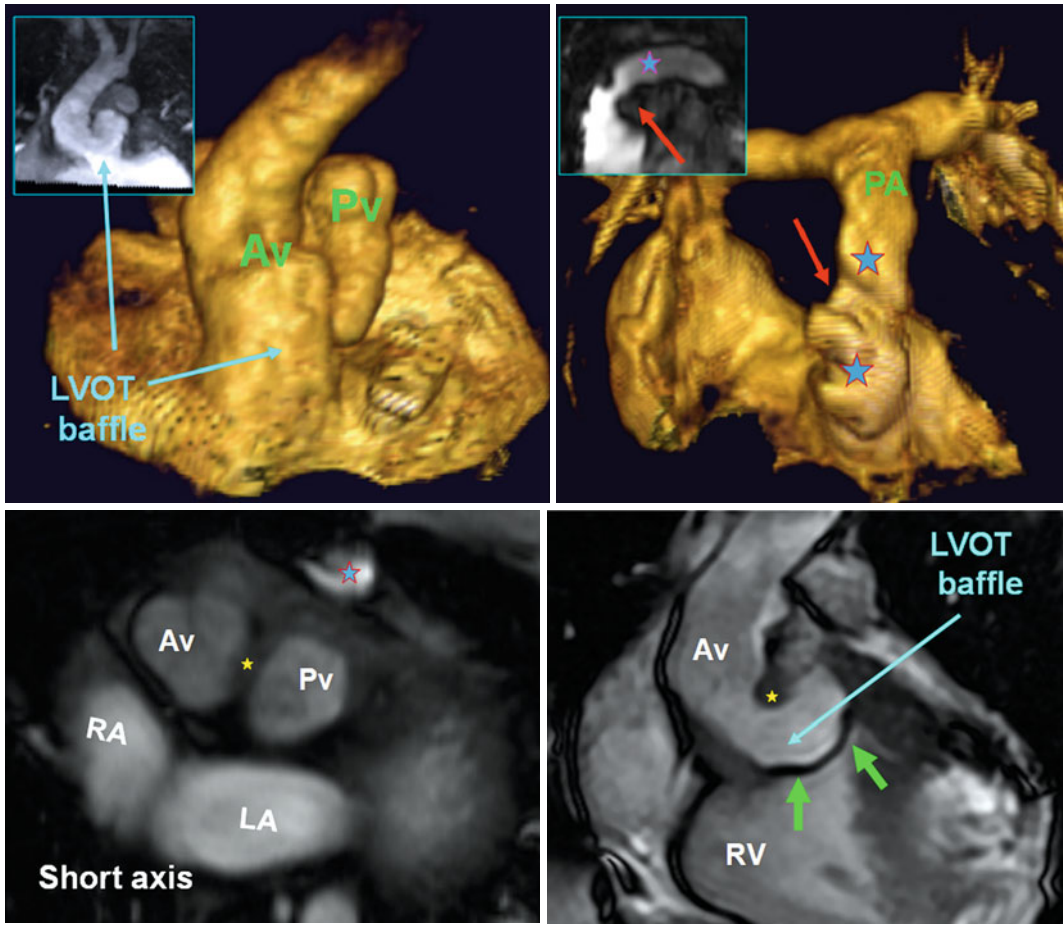

Fig. 7.23 Spectrum of findings in repaired DORV. A 22-year-old male status post Rastelli repair for double outlet right ventricle (DORV). Rastelli repair is performed by an intraventricular tunnel made of a Gore-Tex patch (*green arrows*) to baffle left ventricular blood to the aorta (*blue stars*) and placement of a right ventricular-to-pulmonary artery (*PA*) conduit. RV-to-PA conduit shows mild narrowing (*red arrows*). Note side-by-side position of the aortic (A) and pulmonary (P) valves and the outlet septum between them (*yellow stars*). *RV* right ventricle, *RA* right atrium, *LA* left atrium, *LVOT* left ventricle outflow tract

procedure the pulmonary artery is brought forward anterior to the aorta and the coronary buttons are sutured into the "neoaorta" [61]. Complications can be shown by CT or MRI. These include distortion of the RVOT and pulmonary arteries, neoaortic root dilatation with aortic regurgitation, and rarely coronary artery stenosis [61].

Congenitally Corrected TGA

In congenitally corrected TGA (ccTGA), blood flows in the normal direction but through the "wrong" ventricle (Fig. 7.24c, d). The morphological LV and mitral valve supply the pulmonary circulation, and the morphological RV and tricuspid valve supply the systemic circulation [62, 63]. The most common anatomical arrangement is situs solitus with L-looping of the ventricles and the aorta anterior and leftward of the pulmonary artery [62]. At the earliest sign of deterioration in systemic ventricular function, systemic atrioventricular valve regurgitation should be suspected [64, 65]. Most centers would not recommend a prophylactic double switch procedure for patients without associated abnormalities in whom RV and tricuspid valve function is normal. Regular assessment of ventricular function using cardiac MRI every few years is suggested [64].

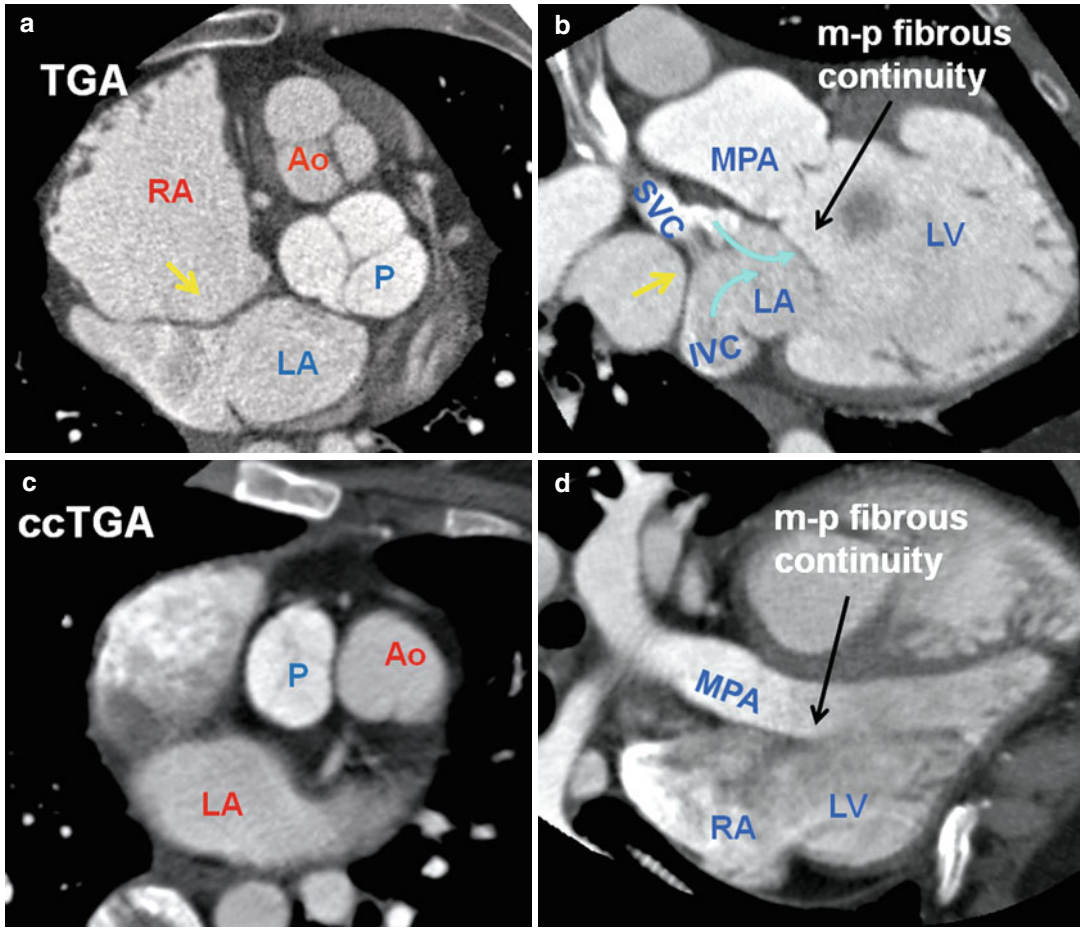

Fig. 7.24 Anatomical features of the outflow tract in transposition of great arteries (TGA) and congenitally corrected malposition of great arteries (ccTGA). (**a**, **b**) TGA status post atrial switch. In TGA the aortic valve (*Ao*) is located anterior to the pulmonary valve (*P*) in most cases, and the great arteries are parallel rather than crossing as they do in the normal heart. The second most common arrangement is with the aorta just anterior to the pulmonary artery. There is fibrous continuity of the mitral and pulmonary valves (m–p continuity). Intra-atrial baffle (*yellow arrows*) shifts deoxygenated blood of the SVC and IVC into the left atrium (*LA*) vestibule, left ventricle (*LV*), and main pulmonary artery (*MPA*). The right ventricle is the systemic ventricle and will be hypertrophied. (**c**, **d**) In ccTGA the ventricles are congenitally inverted with the LV located behind the sternum. The pulmonary (*P*) and aortic (*Ao*) valves are usually side-by-side with the aorta on the left. This anatomical arrangement of great arteries can be rarely seen in TGA (<10 %). The pulmonary artery in ccTGA arises directly from the LV with direct fibrous continuity between the mitral and pulmonary valves. *IVC* inferior vena cava, *RA* right atrium, *SVC* superior vena cava

Truncus Arteriosus

Truncus arteriosus consists of a single arterial trunk giving origin to the pulmonary arteries, the coronary arteries, and the systemic circulation [66]. Several classifications of the common trunk have been proposed on the basis of the origins of the pulmonary arteries [66, 67]. Progressive dilatation of the common trunk as a result of cystic medial necrosis is common. The common trunk usually overrides a large, nonrestrictive VSD resulting from absence of the infundibular septum [18]. It lies between the 2 limbs of the septomarginal trabeculation. The truncal valve is usually tricuspid but can vary between 1 to 6 cusps [18]. The basic repair involves closing the VSD and separating the PAs and attaching them to a valved conduit arising from RVOT [68] (Fig. 7.25). Most patients have reoperation by 10–12 years for conduit replacement (usually because of the small size of the original conduit)

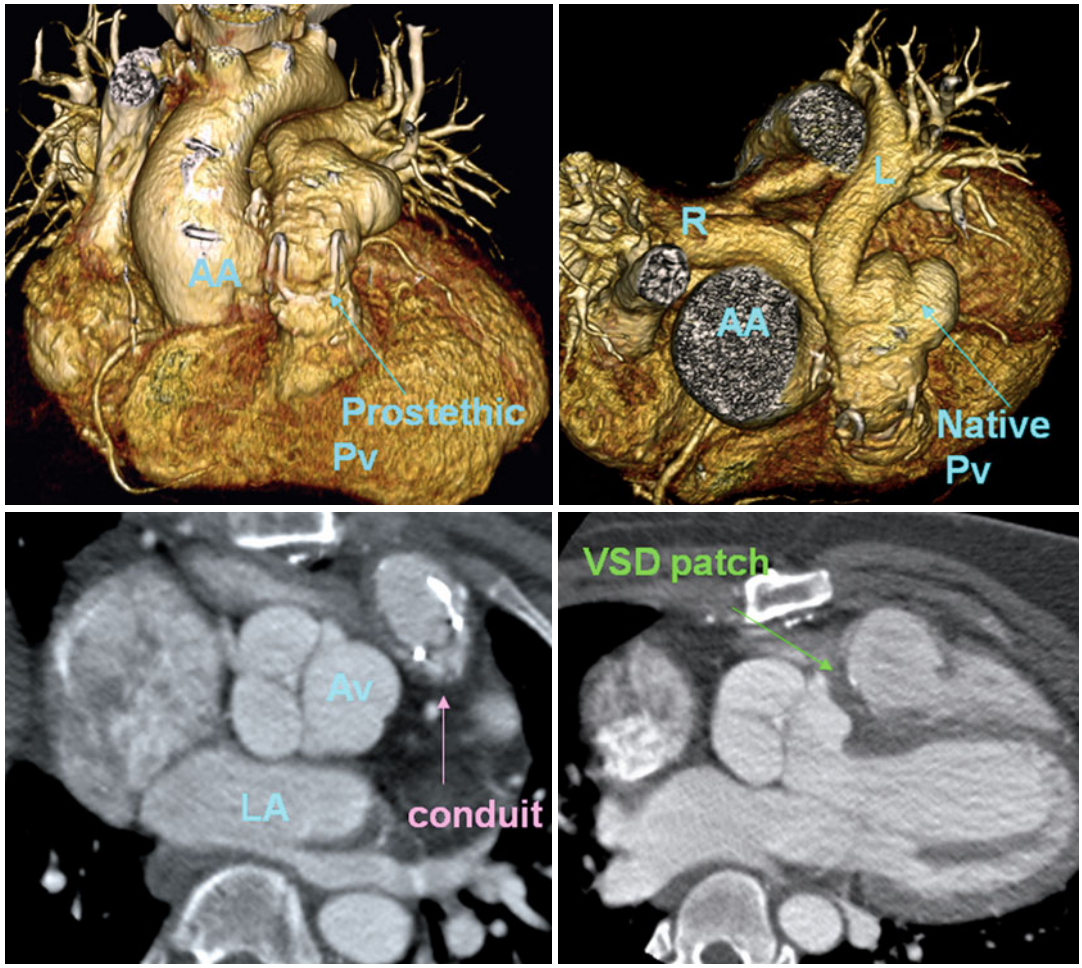

Fig. 7.25 Repaired truncus arteriosus. A prosthetic valve is placed in right ventricle pulmonary artery conduit. Conduit homograft is partially calcified. Sub-truncal VSD patch is shown (*green arrow*). *AA* ascending aorta, *AV* aortic valve, *VSD* ventricular septal defect, *PV* pulmonary valve, *R* right pulmonary artery, *L* left pulmonary artery

or truncal valve replacement because of valvular insufficiency. Truncus arteriosus should not be mistaken with hemitruncus [69]. Hemitruncus is best defined as a condition in which one branch of the pulmonary artery (usually the right) originates from the ascending aorta and the other branch has a normal course arising from a normal main pulmonary artery (Fig. 7.26).

Functional Analysis of the RVOT

Accurate quantification of the RV volume and function has remained clinically challenging despite advances in cardiac imaging. The three-dimensional nature and complex anatomy of the RV make CT and MR ideal tools for assessing its size and function.

Imaging Techniques

Cardiac MRI is an excellent noninvasive imaging modality for RV function analysis and when serial monitoring is necessary (i.e., systemic RV) can be repeated. Unfortunately, in presence of a cardiac pacer, MRI is relatively contraindicated, although this circumstance is changing. In patients with a pacemaker, CT may be a better choice for functional assessment of RVOT

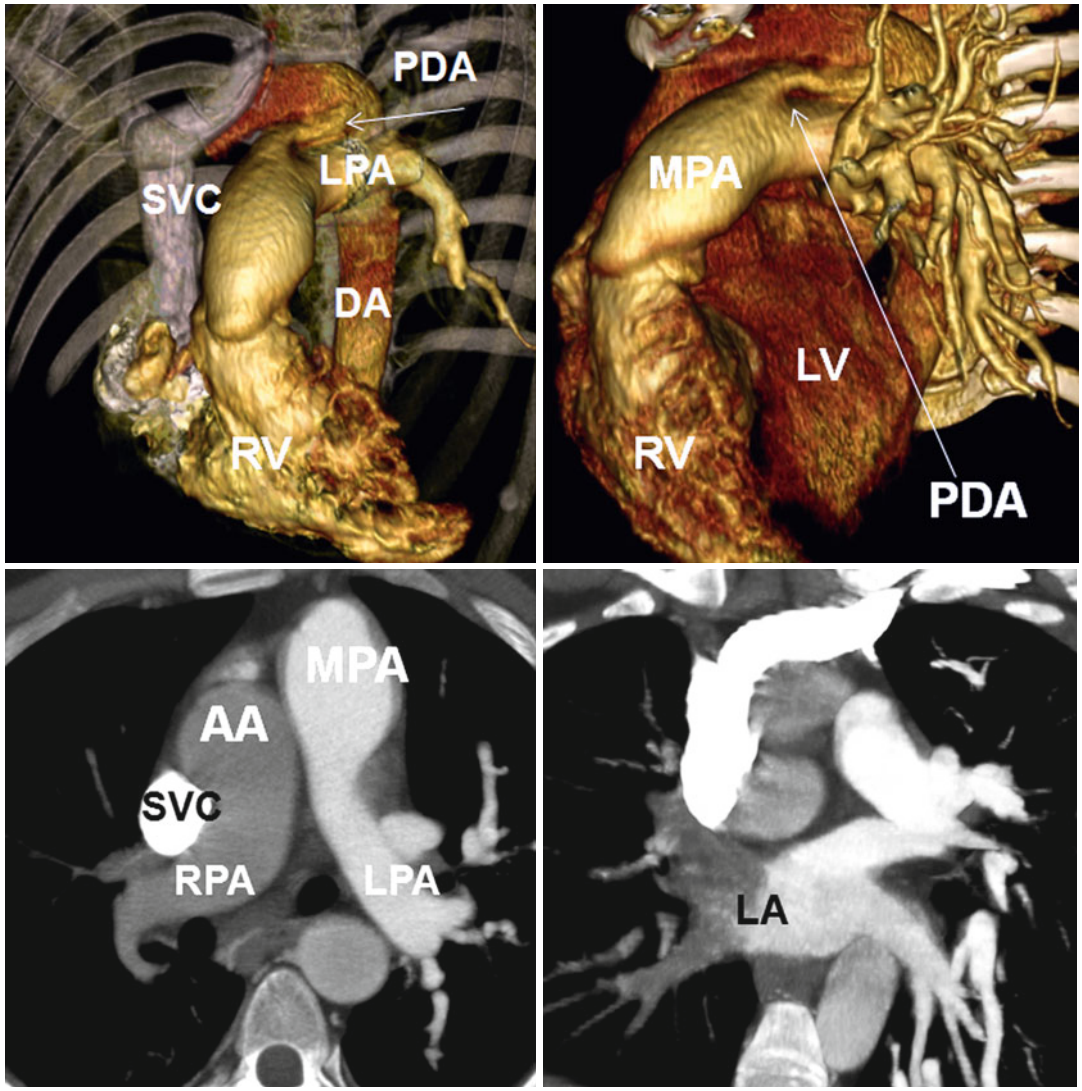

Fig. 7.26 Hemitruncus with anomalous origin of the right pulmonary artery (*RPA*) from the ascending aorta (*AA*). A patent ductus arteriosus (*PDA*) also exists. The CT data is obtained at pulmonary phase and only the right heart is opacified. The left pulmonary artery (*LPA*) originates normally from the main pulmonary artery (*MPA*). Delayed opacification of the RPA as a result of its origin from the aorta has given a double contrast to the left atrium (*LA*) with incomplete filling of the right pulmonary veins. *RV* right ventricle, *LV* left ventricle

especially when evaluation of anatomy and complications related to surgery is also desired and limitations exist for performing echocardiography. Functional MR analysis of the RV and RVOT can be obtained using balanced SSFP cine images [70]. Manual or automated tracing of the endocardial borders of the RV will be performed at end-systolic and end-diastolic phases. The RV volume is then automatically calculated by summation of slice volumes. The process is then repeated by tracing the endocardial borders of the RV inlet or outlet according to the described anatomical landmarks earlier. Using long-axis cross-reference images will help to correctly localize the level of atrioventricular and ventriculoarterial valves as well as the border between the inlet and outlet on short-axis images. Because of RV conduction delay in repaired TOF, the end-diastolic and end-systolic phases of the RV lag the LV. Therefore, images at these phases selected for the

LV volume measurement on short-axis images may not be the same phase for the RV.

Functional analysis can be performed using retrospective ECG-gated cardiac CT. Temporal resolution of CT is not as fast as MRI. With dual source scanners and new reconstruction algorithm, faster temporal resolution (i.e., 83 ms) can be obtained; this way the image quality can be improved by reducing motion artifact [71]. A comprehensive functional assessment of the RV may necessitate MR flow quantification at the level of valves or when RVOT stenosis is suspected on cine images (i.e., double-chambered RV). With new MR phase-contrast techniques, volumetric evaluation of hemodynamics is possible [72]. Care should be taken to avoid sternal wires and surgical clips when localizing the image plane to obtain routine phase-contrast measurements. Both breath hold and free breathing techniques have been used during phase-contrast data collection. It is claimed that pulmonary regurgitant fraction is artificially low in expiratory breath hold technique compared to free breathing or inspiratory breath hold data acquisitions [73].

Arrangement of Muscle Bundles

Architecture of the myocardial strands in the left and right ventricles is fundamentally different (Fig. 7.27). In the relatively thin wall RV circumferential and longitudinal orientations predominate [46, 74, 75]. Subepicardial myofibers retain the circumferential arrangement, and deeper subendocardial myofibers are arranged longitudinally. The hypertrophied RV in TOF can change in architecture to resemble the sandwich pattern (prominent circumferential middle layer) seen in the normal left ventricle (LV) [74]. In the RV, the fibers' orientation can be different in the infundibulum. Myocardial strands are mainly aligned in circular fashion in the subepicardium of the RVOT and form the bulk of the wall [75] (Fig. 7.2). At the subendocardium of the infundibulum, there are longitudinally aligned myofibers, these forming the series of septoparietal trabeculations that branch laterally from the septomarginal trabeculation and may form parallel or crossed strands (Figs. 7.6 and 7.27). These septoparietal trabeculations can be flat or prominent and may be hypertrophied as in pulmonary hypertension, TOF, or pulmonary valve stenosis, contributing to muscular pulmonary subvalvular stenosis (Fig. 7.6).

Regional Differences in Right Ventricular Systolic Function

Global assessment of the RV function is difficult owing to the underlying complex anatomy with the inlet and outlet contracting almost perpendicular to each other. When the overall RV function is taken into account, it is important to mention that the inlet part of the RV has a greater contribution compared with the outlet. The outlet (infundibulum) comprises 20 % of the RV volume and contributes 15 % of the total RV ejection fraction [70]. The conduction in the RV is provided by a single long fascicle and takes time resulting in a peristaltic-like motion with the outlet following the RV inlet by >15 % of the cardiac cycle delay [70]. This pattern can be lost in pulmonary hypertension patients, and all RV components may reach minimum volume simultaneously [76, 77]. Furthermore, RVOT fractional shortening will be reduced early in patients with pulmonary hypertension, while their right ventricular systolic long-axis excursion may remain stable [76] (Fig. 7.28). RVOT fractional shortening is simply calculated as the percentage shortening in RVOT anteroposterior diameter in systole with respect to that in diastole using a three-chamber or axial view. The right ventricular systolic long-axis excursion is the difference between diastolic and systolic lengths of RV measured from the lateral margin of tricuspid ring to the RV apex on a four-chamber view. Using CT data, it is seen that RVOT diameter and cross-sectional area measured during systole are larger in patients with pulmonary hypertension compared with normal subjects, whereas diastolic values are not significantly different [12].

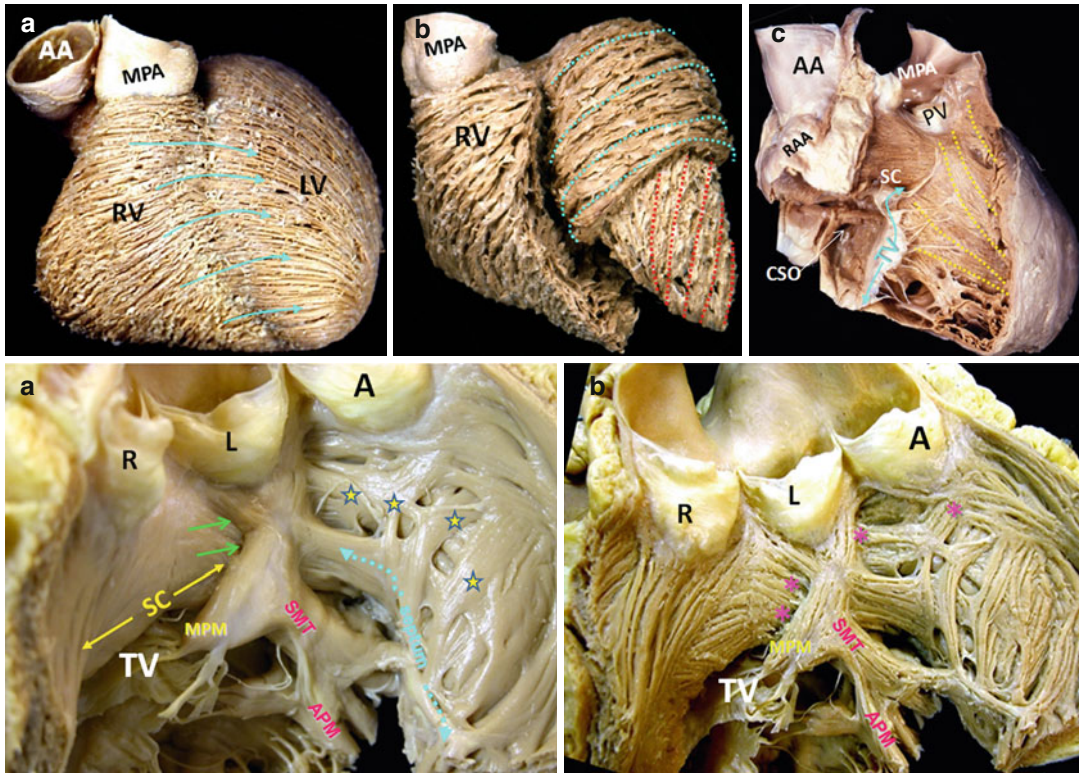

Fig. 7.27 *Upper panel*: (**a**–**c**) These dissections show the change in the myocardial grain, representing the overall oblique or circumferential orientation of the myocardial strands in the epicardial or superficial region (**a**) of the right ventricular walls. Note that there is continuity between the superficial fibers of the right and left ventricle (*arrows*). (**b**) Demonstrates prominent circumferential middle of the left ventricle (*blue dotted lines*) which is absent within the normal right ventricle. (**c**) Demonstrates the deep or subendocardial region in an opened right ventricle (*yellow dotted lines*). This deep region can also be seen in the left ventricle (*red dots*) in image **b**. Note subendocardial myocardial strands are longitudinally or obliquely arranged at right angles with respect to epicardial strands. *RV* Right ventricle, *LV* Left ventricle, *AA* Aorta, *CSO* Coronary sinus orifice, *RAA* Right atrial appendage, *TV* Tricuspid valve (*blue line*), *PV* Pulmonary valve, *MPA* Main pulmonary artery. *Lower panel*: (**a**) Endocardial view of the RVOT. Note that endocardial infundibular sleeve consists of septoparietal trabeculations (*stars*) arising from the septomarginal trabeculation (*SMT*), the medial papillary muscle (*MPM*) and the junction (*green arrows*) between the supraventricular crest (*SC*) shown by (*yellow arrows*), and SMT. The interventricular septum is shown by dotted (*blue line*). (**b**) Same specimen showing the RVOT subendocardial myofibers arrangements. Note the crossing architecture pattern of the myocardial strands between the SMT with the septoparietal trabeculations and supraventricular crest below the pulmonary valve (*asterisks*). *L* left, *A* anterior, *R* right, *TV* tricuspid valve, *APM* anterior papillary muscle

Right Ventricle Outflow Tract Stenosis

RVOT hypertrophy is common in chronic pulmonary valve stenosis and may lead to a fixed or dynamic subvalvular stenosis (Fig. 7.3). RVOT stenosis, which can be due to extrinsic or intrinsic causes, can result in hemodynamic instability and defined as "significant" when the peak right ventricular-to-pulmonary artery systolic gradient exceeds 25 mmHg. Furthermore, significant RVOT stenosis is defined as "fixed" if there is no change in RVOT dimensions during the cardiac cycle and as "dynamic" if RVOT dimensions increase appreciably in diastole [78]. A hypertrophied RV can maintain its function for years, even when RV pressures are near systemic. Symptoms occur at a variable level of valve gradient but usually much later than an RV pressure exceeding 50 % of systemic pressure. Echocardiography is the best modality for diagnosis and grading of stenosis. MR and CT can

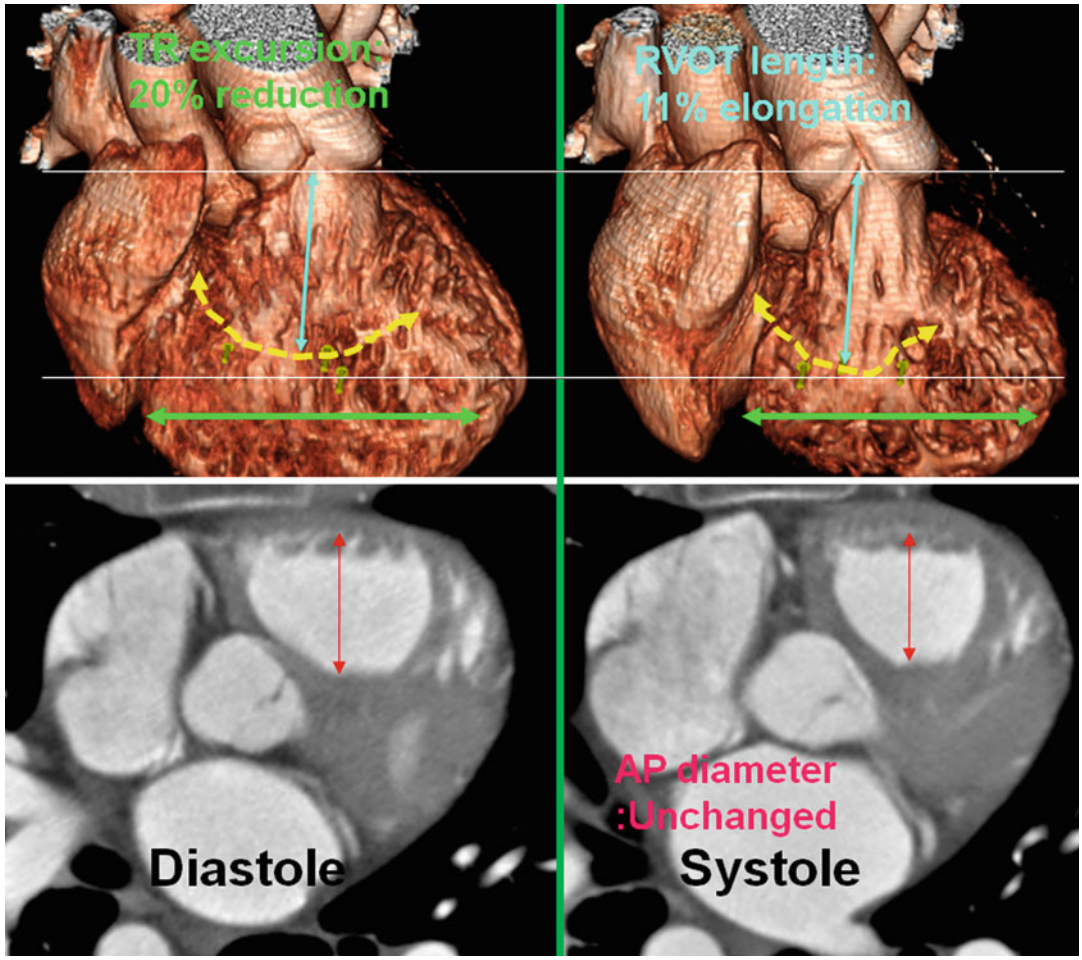

Fig. 7.28 Right ventricle outflow tract (*RVOT*) function in pulmonary hypertension. In pulmonary hypertension, compared to normal, tricuspid ring (*TR*) excursion (*green arrows*) only mildly decreases, but the RVOT anteroposterior diameter (*AP*) remains unchanged or mildly contracted in systole compared to diastole (*red arrows*). AP shortening fraction is used as one of the early parameters that will change in pulmonary hypertension. Note the length of RVOT (*blue arrows*) is not only changed but mildly increased in systole compared to diastole. *Yellow curve* shows the beginning of the RVOT

also provide valuable information on valve mobility, RV size and function, the presence of post-stenotic dilatation, locating a pulmonary subvalvular stenosis, and associated pathologies [79] (Fig. 7.29).

RVOT and RV Function in Repaired TOF

Evaluation of the regional adaptation of three components of the morphological RV to different conditions of loading by imaging techniques can be important especially in repaired congenital heart disease. The apical trabecular component provides the major ejectile momentum of the ventricle, and its function is maintained in patients with slight-to-moderate ventricular dysfunction. The outlet part, in contrast, shows a consistently and markedly decreased ejection fraction irrespective of the nature of the overload. In post-repair TOF, although the surgical subjects have lower RVOT ejection fraction and higher indexed volumes, most show reserved inlet ejection fraction [80]. The pulmonary infundibulum may be essential for right ventricular ejection and for maintaining pulmonary valve competence.

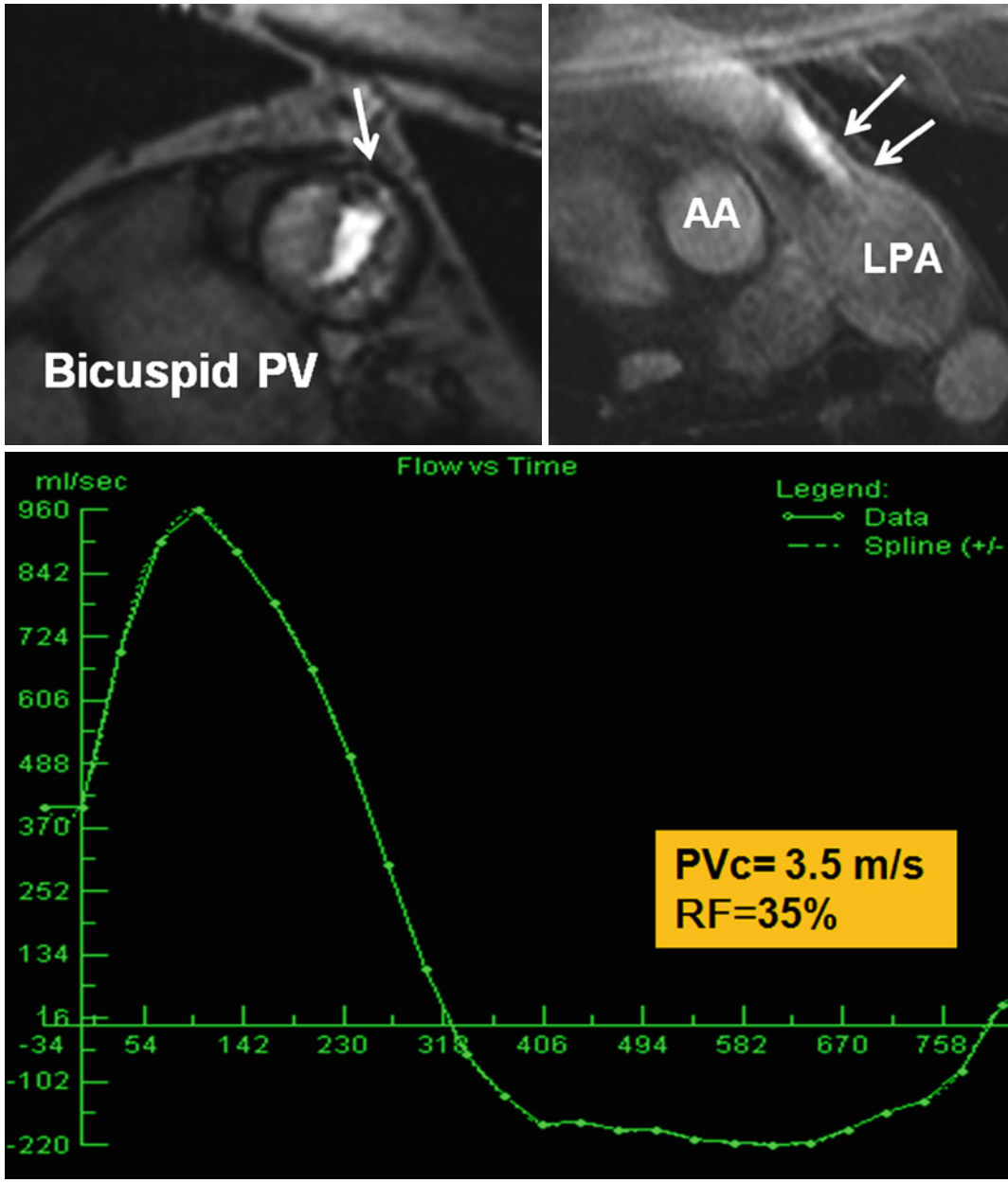

Fig. 7.29 Transaxial and long-axis MRI of a stenotic bicuspid pulmonary valve (PV) (*arrow*) with jet flow (*double arrows*) and post-stenotic dilatation of the left pulmonary artery (*LPA*) are shown in upper row. Systolic flow turbulence and increased peak velocity (*PVc*) of 3.5 m/s by phase velocity mapping were seen. Flow profile, mL/s versus time (ms), is shown. There was moderate (free) pulmonary valve insufficiency with regurgitant fraction (*RF*) 35 %. The regurgitant fraction is defined as regurgitant volume divided by the stroke volume. *AA* ascending aorta

Transannular patching gives excellent relief of the RVOT obstruction but invariably causes pulmonary insufficiency, hypokinesis and aneurysm of the RVOT, and fibrosis (Fig. 7.30). Surgical attempts to preserve pulmonary valve competence by limiting the patching to the ventricular area below the pulmonary valve may not protect patients from the late deleterious consequences

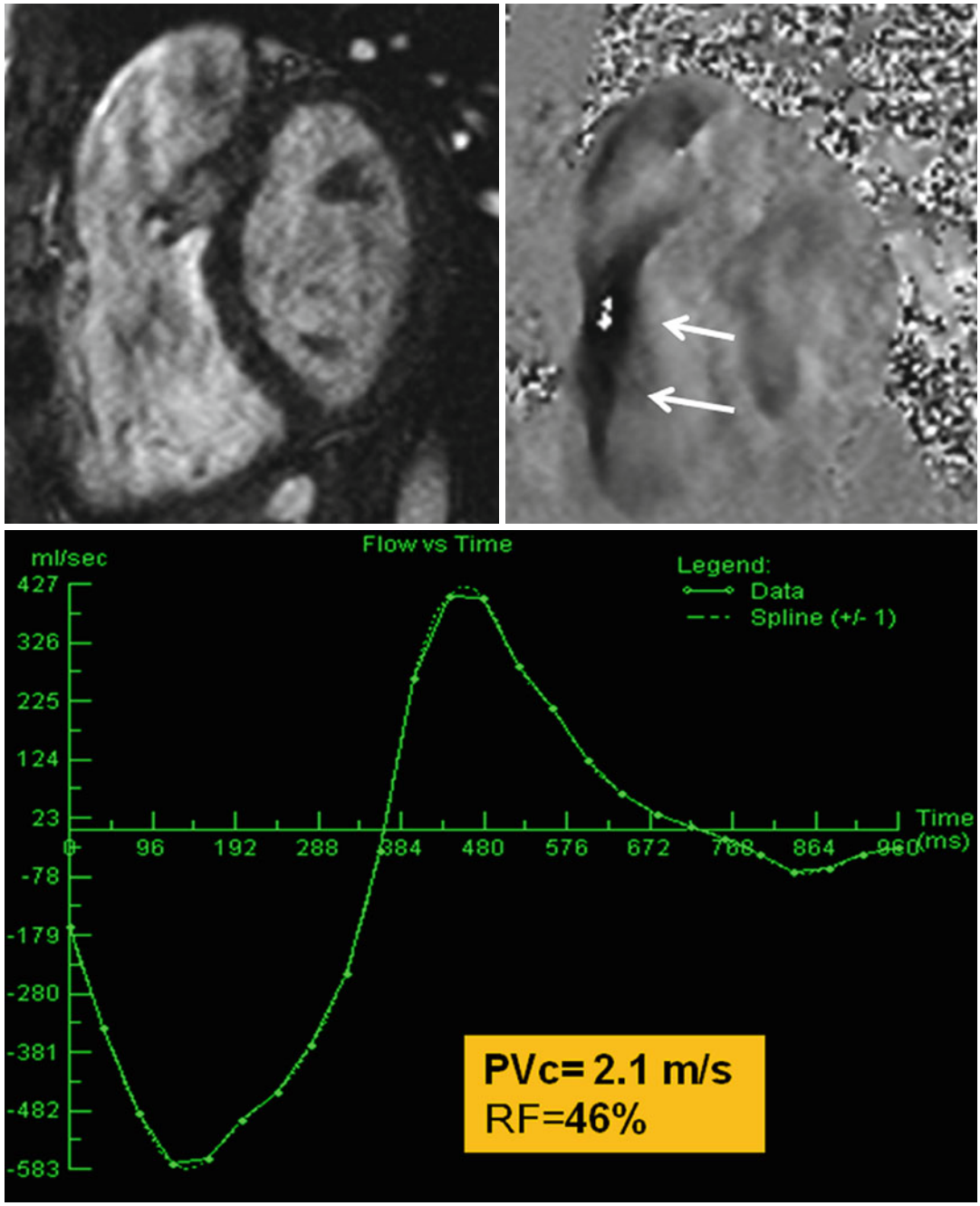

Fig. 7.30 Post-repaired tetralogy of Fallot showing free flow regurgitation at pulmonary valve level best shown on phase image (*arrows*). Flow profile, mL/s versus time (ms), shows moderate to severe pulmonary valve insufficiency with a regurgitant fraction (*RF*) of 46 %. Peak velocity (*PVc*) was 2.1 m per second (m/s). Time-flow volume curve is recorded reverse with forward flow shown in negative direction. Note mild late diastolic forward flow due to forced atrial contraction related to impaired relaxation of the right ventricle. Documentation of severe pulmonary regurgitation, exercise limitation, and excessive right ventricular dilatation, defined by a RV/LV ratio of 2:1 by MRI, has been used as criteria for valve replacement

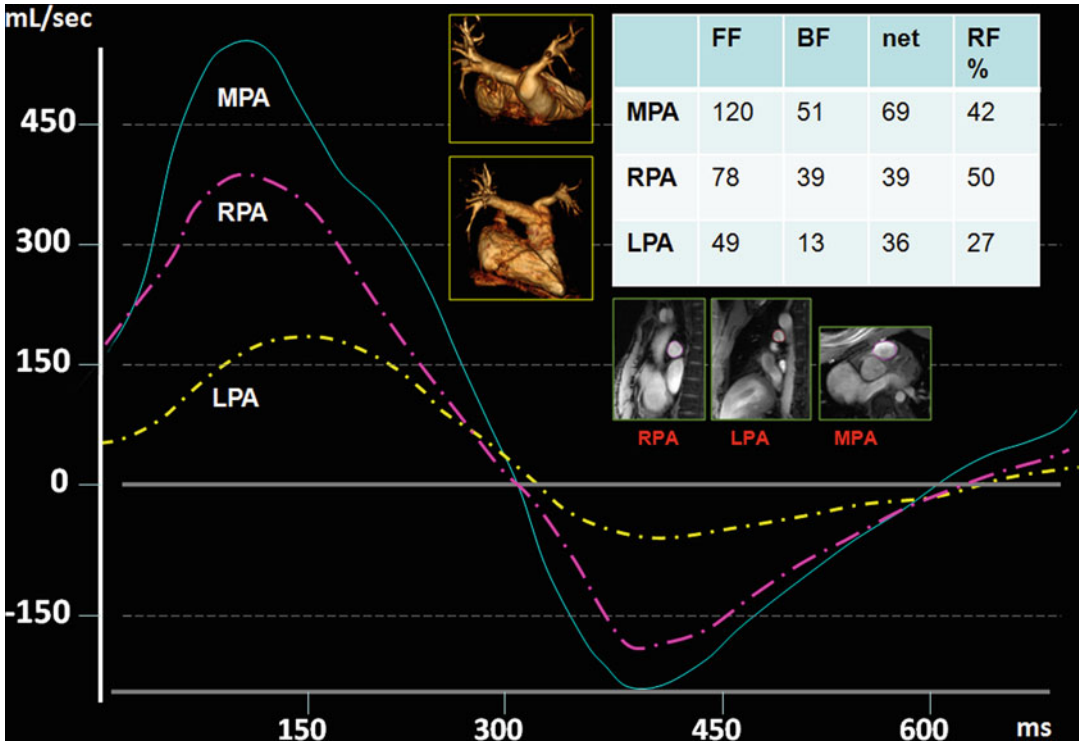

	FF	BF	net	RF %
MPA	120	51	69	42
RPA	78	39	39	50
LPA	49	13	36	27

Fig. 7.31 Time-flow curves, phase-contrast magnitude views, and volume-rendered MR angiography of pulmonary arteries are shown. Status after tetralogy of Fallot repair with larger right pulmonary artery (*RPA*) compared to the left pulmonary artery (*LPA*). Differential regurgitant fraction (*RF*) of the RPA and LPA is shown. Despite larger size of RPA, the net flow to both RPA and LPA is almost equal due to larger RF of the RPA. The elevated RPA–RF may be related to elevated right-sided pulmonary vascular resistance. *BF* backward flow, *MPA* main pulmonary artery, *FF* forward flow

of RV dilatation [81]. It is possible that the source of global RV dysfunction in repaired TOF is because of the dyskinesis of the infundibulum and dyssynchrony of RV contraction [82]. There is a close relationship between the degree of pulmonary insufficiency and RV diastolic dimensions and stroke volume. Adverse ventricular–ventricular interaction could be an important mechanism in which RV dilatation and dysfunction lead to LV dysfunction. In phase-contrast analysis of the outflow tract regurgitation, both regurgitant volume and fraction values are equally important and should be reported [83]. Regurgitant fraction (regurgitant volume x 100/forward flow volume, in %) can be artificially high in the presence of low RV systolic function but modest amount of regurgitant volume. It is also important to measure differential regurgitant fraction of the left and right pulmonary artery branches. In the absence of stenosis or marked dilatation of one vessel, regurgitant fraction is usually higher on the left side and may be related to increased peripheral vascular resistance [84] (Fig. 7.31). Indications of pulmonary valve replacement include in moderate to severe insufficiency, RV/LV diameter or end-diastolic volume ratio >2, RV end-diastolic volume index >150–160 mL/m^2, RV and/or LV dysfunction, and large RVOT aneurysm. Cardiac MR is the ideal method for longitudinal follow-up in patients with repaired TOF. Following percutaneous valve replacement, end-diastolic and end-systolic volumes decrease by 30–40 %, and tricuspid regurgitation improves, although global RV systolic function (measured as ejection fraction) remains unchanged. The RV size may not return to normal in preoperative end-diastolic volume index >170 mL/m^2 [79].

Detailed information about three-dimensional (3D) hemodynamics and flow alterations occurring in the RVOT and the entire pulmonary vascular system in post-repair TOF are important before valve surgery. Time-resolved 3D phase-contrast MRI with three-directional velocity encoding, also known as flow-sensitive 4D-MRI, has introduced as a valuable method for comprehensive analysis of RVOT function [72]. Routine phase-contrast methods can be used to quantify differential pulmonary flow in order to assess the significance of a branch pulmonary stenosis. A severe discrepancy in pulmonary blood flow (>35 %) requires treatment of the branch pulmonary stenosis before repair of the RVOT [79]. Identification of residual intracardiac shunt with cardiac MR is also important before percutaneous pulmonary valve replacement. For example, in the presence of a moderate pulmonary regurgitation (35 % regurgitant fraction) and RV dilatation, even a small shunt (i.e., <1.3 pulmonary-to-systemic flow ratio) can be problematic and should be treated.

RVOT Function in Systemic RV

In patients with ccTGA and post-atrial switch TGA, the RV functions as the systemic pumping chamber. In these condition the infundibulum is very short and underdeveloped, and RV dysfunction and tricuspid regurgitation are common (Fig. 7.24). A shift in the systemic RV myostructure from longitudinal to circumferential shortening is seen as an adaptive response to the systemic load when compared with the normal RV. However, in contrast to the normal LV, ventricular torsion is essentially absent and strain rate is reduced [85–87]. It seems that ventricular hypertrophy, the design of the respective atrioventricular valve, the lack of torsion, reduced strain rate, and possibly myocardial ischemia might be factors responsible for accelerated failure of the systemic RV [86–89]. Generally, the goals of MRI after an atrial switch procedure include evaluations of the function and size of the ventricles, careful assessment of the intra-atrial baffle for leak and stenosis, atrioventricular valves for regurgitation, and outflow tracts for obstruction. The number of adult patients with ccTGA who need CT or MRI for early detection of complications has been increasing, due to better imaging techniques as well as increasing life expectancy of these patients. A small percentage of patients with ccTGA have no intracardiac defect and may remain asymptomatic until age 40–50. The role of MRI or CT in these cases is mainly in the assessment of systemic RV function and associated tricuspid regurgitation. CT may be advantageous over MRI in delineation of the coronary anatomy origin before surgery or in patients with an endocardial pacer.

RVOT Myocardial Scar

Detection of myocardial scar in MR or CT exam of adult congenital heart malformations is not uncommon and most of the time is located at areas of patch repairs or ventriculostomy (Fig. 7.32). Scar tissue and/or patch material in the RVOT can adversely affect RV mechanics after TOF repair. In post-repair TOF, regional functional abnormalities and hyperenhancement are most common in the RVOT [90]. Hyperenhancement frequently extends to the anterior RV free wall and neighboring segments. Typical sites of hyperenhancement include anterior wall of RVOT (99 %), VSD patch area (98 %), moderator band (24 %), site of apical vent insertion in the LV (48 %), and inferior (80 %) and superior (24 %) insertion points [90]. Delayed myocardial enhancement in the systemic RV (TGA with atrial switch and ccTGA) is not uncommon and has direct correlation with patient age, myocardial wall thickness, and end-systolic volume of the RV and may be associated with cardiac arrhythmia and sudden death [85]. Enhancement patterns include localized full-thickness RV anterior wall enhancement, small patchy areas of enhancement, and VSD closure site. It is important to remember that in the presence of subendocardial or transmural enhancement in a vascular territory, coronary artery disease should be excluded. Enhancement at RV free-wall insertion to interventricular septum is a common finding and seems more characteristic of continuous pressure overload [85]. RVOT wall enhancement in arrhythmogenic right ventricular cardiomyopathy/dysplasia (ARVD/C) is not uncommon [91].

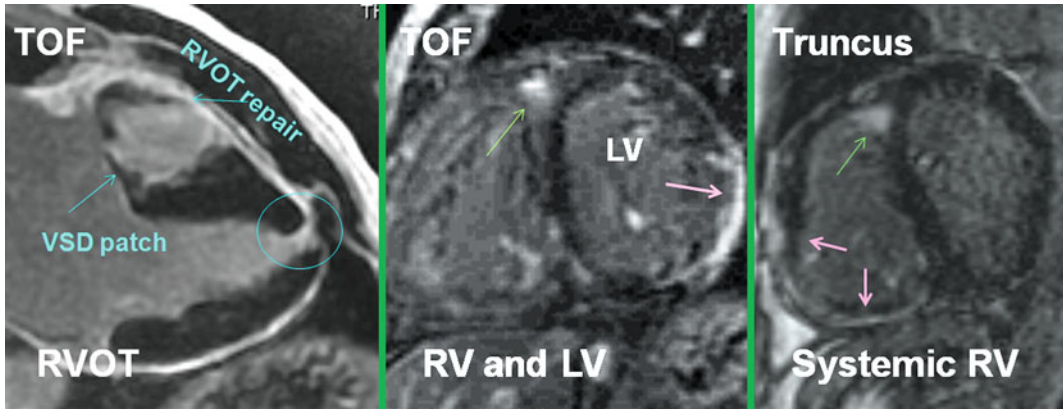

Fig. 7.32 Common locations of RVOT myocardial scars. In tetralogy of Fallot (*TOF*), scars at surgical repair site, around VSD patch, and ventriculostomy site are the most common locations. The right ventricle (*RV*) free wall can easily be involved in systemic RV (*red arrows*) as shown in this 41-year-old patient with truncus arteriosus and single ventricle. Enhancing sites at the RV free-wall insertion sites to the septum are benign findings (*green arrows*). The left ventricle wall is involved in middle image (*red arrow*). Scars in RVOT may predispose to cardiac arrhythmias. *LV* left ventricle, *VSD* ventricular septal defect

RVOT and Cardiac Arrhythmias

The RVOT is generally a common source of cardiac arrhythmias. The embryonic OFT consists of slowly conducting tissue until it is incorporated into the ventricles and develops rapid conducting properties. It is suggested [92] that remnants of the embryonic OFT phenotype and expression profile in the adult RVOT determine the electrophysiological and structural characteristics that make the RV more vulnerable for arrhythmias. Patients with TOF have higher rate of atrial and ventricular arrhythmias [93]. Potential risk factors for ventricular tachycardia (VT) include aneurysmal dilation of the RVOT, RV dilatation, and pulmonary regurgitation. Ventricular arrhythmias are usually localized to the RVOT act, and the scars at infundibulotomy, VSD patch repair, or ventriculostomy may increase the risk [93].

Morphological changes of the RV free wall are described in patients with idiopathic RVOT tachycardia using MRI including fat deposition, wall thinning, saccular aneurysm, and dyskinesis in up to 60–65 % of cases [94, 95]. VT is also a common complication in patients with arrhythmogenic right ventricular cardiomyopathy/dysplasia (ARVD/C) and may arise from the RVOT [96]. Currently, RVOT ventricular tachycardia ablation is guided by traditional electrophysiologic and electroanatomic methods. CT and MR can help in demonstrating myocardial scar, vascular integrity of the RVOT, and better localizing the source of arrhythmia by image fusion techniques. The relationship of coronaries with RVOT can nicely be depicted with CT scan. When distance between the coronary arteries and the ablation sites is found to be less than 5 mm, cryoablation or 4-mm-tip catheters may be considered to avoid short- and long-term damage to the coronary arteries [97]. Fat deposition in the RV and RVOT wall is not limited to idiopathic VT or ARVD [98]. It is seen in 25 % asymptomatic general population and increases with age [99, 100]. Fat can develop at the site of any myocardial scar including the site of surgery (i.e., Ross procedure). The relation of RV fat with RV function or OFT arrhythmias is not clear.

Rare Causes of RVOT Obstruction

Extrinsic RVOT obstruction has been recognized as a possible cause of hemodynamic instability after cardiac surgery and should be reported in postoperative chest CT scans [81]. Extrinsic compression can occur from an aortic or pulmonary artery aneurysm or postoperative mediastinal hematoma [101]. Intrinsic obstruction is

mainly related to congenital heart disease. Hypertrophic cardiomyopathy and ventricular non-compaction may rarely cause RVOT obstruction [102, 103].

Post-Ross Outflow Tract

The Ross procedure is aortic valve replacement with the autologous pulmonary valve which eliminates problems with aortic prosthetic valve or allograft replacements especially in children [104]. It is a procedure of choice in children with severe anomaly of the aortic valve and/or left ventricular outflow tract obstruction [105]. The main concern after surgery is dilatation of the neoaortic root leading to progression of aortic regurgitation, especially in the settings of geometric mismatch of the aortic and pulmonary roots and regurgitant valve (Fig. 7.33).

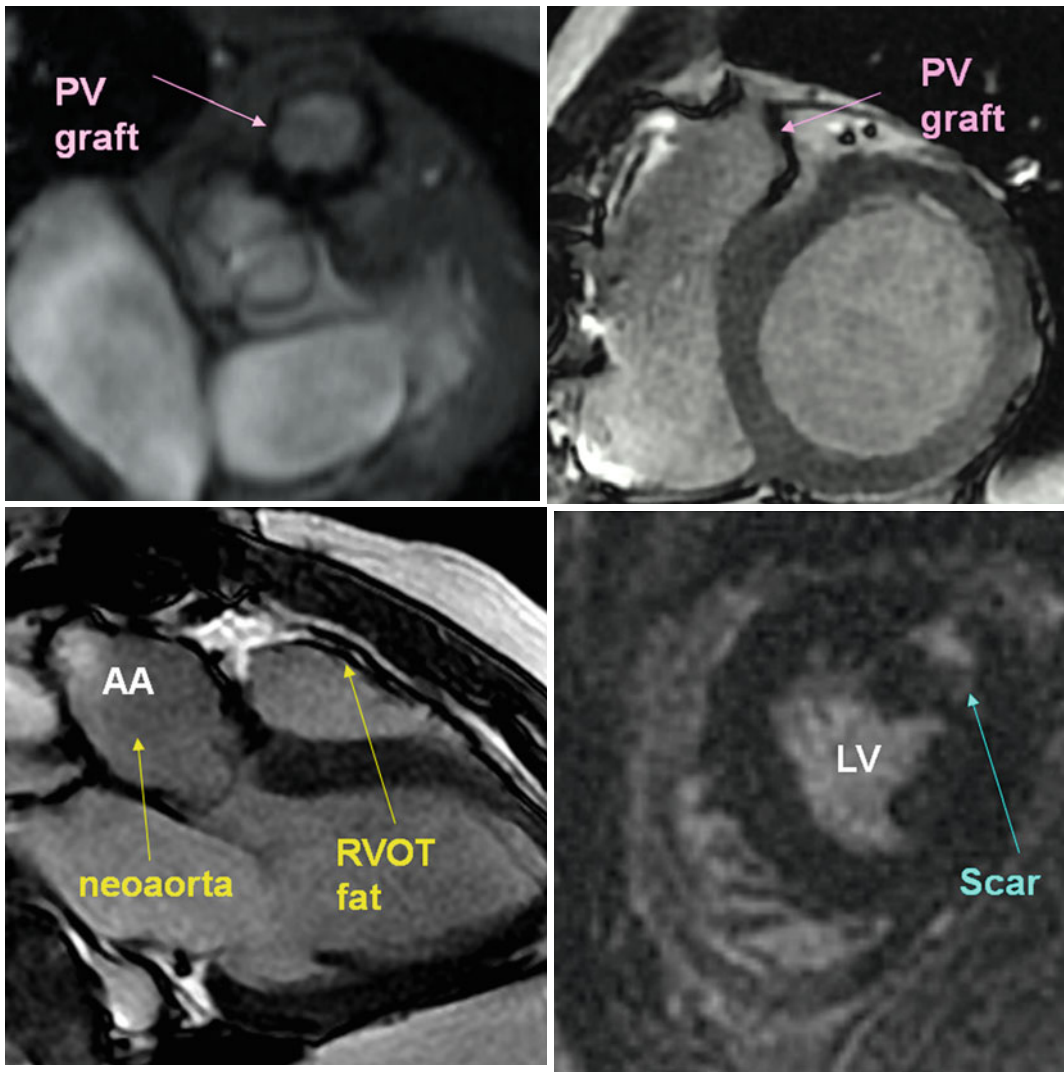

Fig. 7.33 A 29-year-old male with congenital heart disease, status post Ross procedure, and pulmonary homograft revision. MR images show dilated aortic root (pulmonary autograft) and severe aortic regurgitation with regurgitant fraction of 45 %. The bioprosthetic pulmonary valve (*PV*) showed mild stenosis and regurgitation. Note fatty degeneration of right ventricle outflow tract (*RVOT*) and intramyocardial scar of the left ventricle (*LV*). *AA* ascending aorta

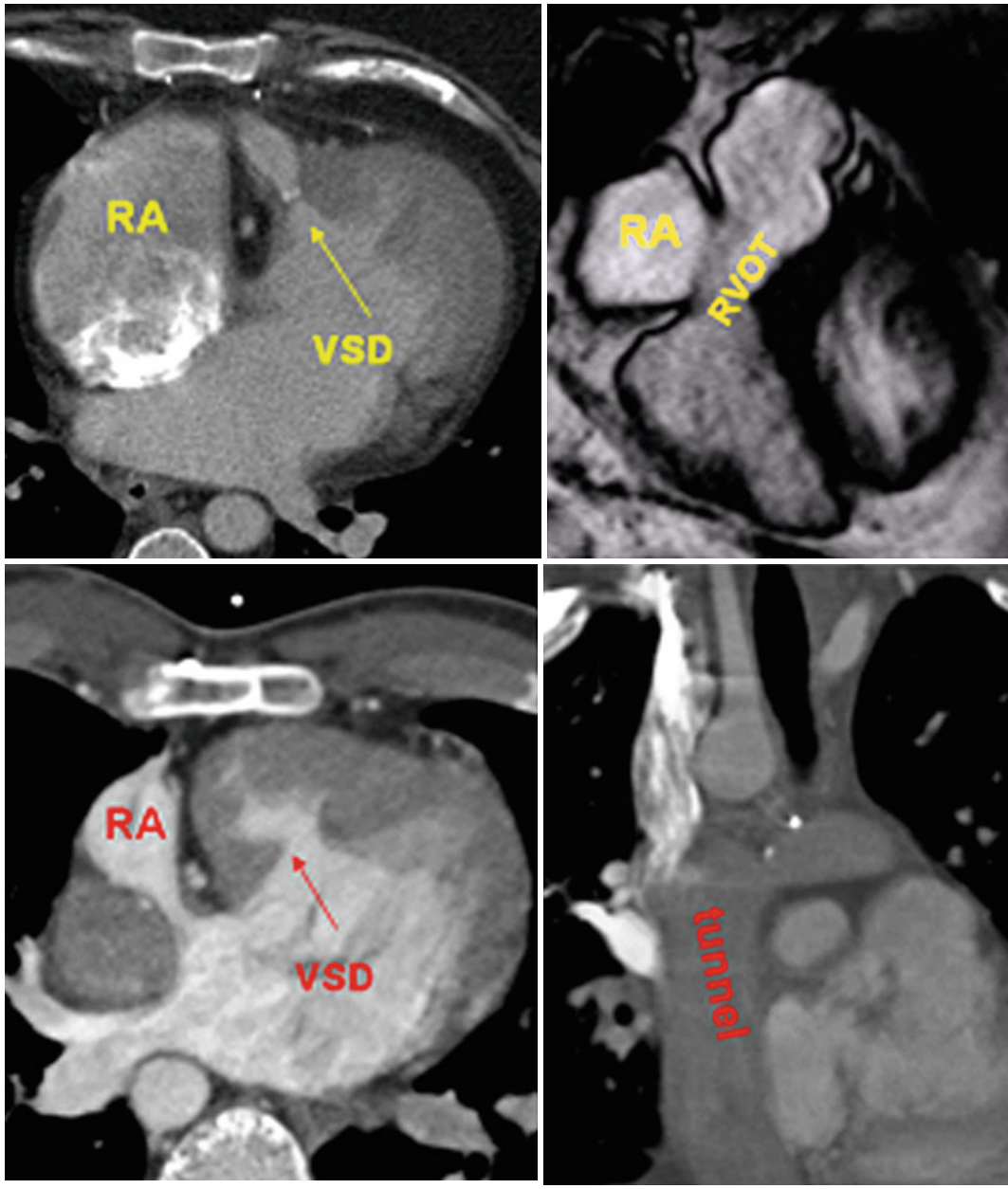

Fig. 7.34 Axial and coronal CT images. Bjork surgery showing right atrium (*RA*) to RVOT (*upper row*) versus total cavopulmonary connection with extracardiac lateral Fontan tunnel (*bottom*) for tricuspid atresia. Note markedly dilated right RA in Bjork. *RV* right ventricle, *RVOT* right ventricle outflow tract, *VSD* ventricular septal defect

Problems with the homograft used in reconstruction of the RVOT are not usually significant, although mild regurgitation is common and up to about 20 % of patients tend to have mild gradients which can be relieved with balloon dilatation [105].

Bjork Surgery

The procedure involves right atrium to RV connection and has been done in the past for tricuspid atresia (Fig. 7.34). The usual surgical approach for tricuspid atresia is Blalock–Taussig

shunt or pulmonary artery band soon after birth, followed by Glenn surgery (bidirectional cavopulmonary shunt) at 3–6 months of age, and finally Fontan surgery at 2–3 years of age [106].

Conclusion

Detailed information about the embryology and anatomy of RVOT provides a better understanding of the spectrum of diseases involving this important area and helps to narrow differential diagnosis of malformations involving this important structure. CT and MR can provide most of the data regarding anatomical, functional, and pathological changes of the RVOT.

References

1. Waldo KL, Kumiski DH, Wallis KT, et al. Conotruncal myocardium arises from a secondary heart field. Development. 2001;128:3179–88.
2. Kirby ML. Cardiogenic fields and heart tube formation. In: Kirby ML, editor. Cardiac development. 1st ed. Oxford/New York: Oxford University Press; 2007. p. 21–35.
3. Kelly RG, Brown NA, Buckingham ME. The arterial pole of the mouse heart forms from Fgf10-expressing cells in pharyngeal mesoderm. Dev Cell. 2001;1:435–40.
4. Waldo KL, Hutson MR, Ward CC, et al. Secondary heart field contributes myocardium and smooth muscle to the arterial pole of the developing heart. Dev Biol. 2005;281:78–90.
5. Webb S, Qayyum SR, Anderson RH, Lamers WH, Richardson MK. Septation and separation within the outflow tract of the developing heart. J Anat. 2003;202(4):327–42.
6. Rana MS, Horsten NCA, Tesink-Taekema S, Lamers WH, Moorman AFM, van den Hoff MJB. The trabeculated right ventricular free wall in the chicken heart forms by ventricularization of the myocardium initially forming the outflow tract. Circ Res. 2007;100:1000–7.
7. van den Hoff MJB, Moorman AFM, Ruijter JM, et al. Myocardialization of the cardiac outflow tract. Dev Biol. 1999;212:477–90.
8. Waldo KL, Hutson MR, Stadt HA, Zdanowicz M, Zdanowicz J, Kirby ML. Cardiac neural crest is necessary for normal addition of the myocardium to the arterial pole from the secondary heart field. Dev Biol. 2005;281:66–77.
9. Restivo A, Piacentini G, Placidi S, Saffirio C, Marino B. Cardiac outflow tract: a review of some embryogenetic aspects of the conotruncal region of the heart. Anat Rec A Discov Mol Cell Evol Biol. 2006;288(9):936–43.
10. Bajolle F, Zaffran S, Kelly RG, et al. Rotation of the myocardial wall of the outflow tract is implicated in the normal positioning of the great arteries. Circ Res. 2006;98(3):421–8.
11. Hoffman JI, Kaplan S. The incidence of congenital heart disease. J Am Coll Cardiol. 2002;39:1890–900.
12. Revel MP, Faivre JB, Remy-Jardin M, Delannoy-Deken V, Duhamel A, Remy J. Pulmonary hypertension: ECG-gated 64-section CT angiographic evaluation of new functional parameters as diagnostic criteria. Radiology. 2009;250(2):558–66.
13. Kerl JM, Ravenel JG, Nguyen SA, et al. Right heart: split-bolus injection of diluted contrast medium for visualization at coronary CT angiography. Radiology. 2008;247(2):356–64, 57.
14. Saremi F, Kang J, Rahmanuddin S, Shavelle D. Assessment of post-atrial switch baffle integrity using a modified dual extremity injection cardiac computed tomography angiography technique. Int J Cardiol. 2013;162(2):e25–7.
15. Ho SY, Nihoyannopoulos P. Anatomy, echocardiography, and normal right ventricular dimensions. Heart. 2006;92 Suppl 1:i2–13.
16. Haddad F, Hunt SA, Rosenthal DN, Murphy DJ. Right ventricular function in cardiovascular disease, part I: anatomy, physiology, aging, and functional assessment of the right ventricle. Circulation. 2008;117(11):1436–48.
17. Anderson RH, Jacobs ML. The anatomy of tetralogy of Fallot with pulmonary stenosis. Cardiol Young. 2008;18 Suppl 3:12–21.
18. Bashore TM. Adult congenital heart disease: right ventricular outflow tract lesions. Circulation. 2007;115(14):1933–47.
19. Alva C, Ho SY, Lincoln CR, Rigby ML, Wright A, Anderson RH. The nature of the obstructive muscular bundles in double-chambered right ventricle. J Thorac Cardiovasc Surg. 1999;117(6):1180–9.
20. Loukas M, Klaassen Z, Tubbs RS, et al. Anatomical observations of the moderator band. Clin Anat. 2010;23(4):443–50.
21. Loukas M, Tubbs RS, Louis Jr RG, et al. An endoscopic and anatomical approach to the septal papillary muscle of the conus. Surg Radiol Anat. 2009;31(9):701–6.
22. Hansen MW, Merchant N. Images in cardiovascular medicine. Vieussens' ring: combining computed tomography coronary angiography and magnetic resonance imaging in assessing collateral pathways. Circulation. 2006;114(16):e545–6.
23. Saremi F, Goodman G, Wilcox A, Salibian R, Vorobiof G. Coronary artery ostial atresia: diagnosis of conotruncal anastomotic collateral rings using CT angiography. JACC Cardiovasc Imaging. 2011;4(12):1320–3.
24. Li J, Soukias ND, Carvalho JS, Ho SY. Coronary arterial anatomy in tetralogy of Fallot: morphological and clinical correlations. Heart. 1998;80(2):174–83.

25. Milo S, Fiegel A, Shem-Tov A, Neufeld HN, Goor DA. Hour-glass deformity of the pulmonary valve: a third type of pulmonary valve stenosis. Br Heart J. 1988;60(2):128–33.
26. Stamm C, Anderson RH, Ho SY. Clinical anatomy of the normal pulmonary root compared with that in isolated pulmonary valvular stenosis. J Am Coll Cardiol. 1998;31(6):1420–5.
27. Berdajs D, Lajos P, Zund G, Turina M. The quadricuspid pulmonary valve. Its importance in the Ross procedure. J Thorac Cardiovasc Surg. 2003;125:198–9.
28. Warnes CA, Williams RG, Bashore TM, et al. ACC/AHA 2008 guidelines for the management of adults with congenital heart disease: a report of the American college of cardiology/American Heart Association Task Force on Practice Guidelines (writing committee to develop guidelines on the management of adults with congenital heart disease). Circulation. 2008;118:e714–833.
29. Kan JS, White Jr RI, Mitchell SE, Gardner TJ. Percutaneous balloon valvuloplasty: a new method for treating congenital pulmonary valve stenosis. N Engl J Med. 1982;307:510–4.
30. Kanter KR, Budde JM, Parks WJ, et al. One hundred pulmonary valve replacements in children after relief of right ventricular outflow tract obstruction. Ann Thorac Surg. 2002;73:1801–6.
31. Becker AE, Connor M, Anderson RH. Tetralogy of Fallot: a morphometric and geometric study. Am J Cardiol. 1975;35:402–12.
32. Howell CE, Ho SY, Anderson RH, Elliott MJ. Variations within the fibrous skeleton and ventricular outflow tracts in tetralogy of Fallot. Ann Thorac Surg. 1990;50:450–7.
33. Tan JL, Davlouros PA, McCarthy KP, Gatzoulis MA, Ho SY. Intrinsic histological abnormalities of aortic root and ascending aorta in tetralogy of Fallot: evidence of causative mechanism for aortic dilatation and aortopathy. Circulation. 2005;112:961–8.
34. Bédard E, McCarthy KP, Dimopoulos K, Giannakoulas G, Gatzoulis MA, Ho SY. Structural abnormalities of the pulmonary trunk in tetralogy of Fallot and potential clinical implications: a morphological study. J Am Coll Cardiol. 2009;54(20):1883–90.
35. Ibrahim T, Dennig K, Schwaiger M, Schomig A. Images in cardiovascular medicine: assessment of double chamber right ventricle by magnetic resonance imaging. Circulation. 2002;105:2692–3.
36. Oliver JM, Garrido A, Gonzalez A, et al. Rapid progression of midventricular obstruction in adults with double-chambered right ventricle. J Thorac Cardiovasc Surg. 2003;126:711–7.
37. Hachiro Y, Takagi N, Koyanagi T, Morikawa M, Abe T. Repair of double-chambered right ventricle: surgical results and long-term follow-up. Ann Thorac Surg. 2001;72:1520–2.
38. Tirilomis T, Friedrich M, Zenker D, Seipelt RG, Schoendube FA, Ruschewski W. Indications for reoperation late after correction of tetralogy of Fallot. Cardiol Young. 2010;20(4):396–401.
39. Shebani SO, McGuirk S, Baghai M, et al. Right ventricular outflow tract reconstruction using Contegra valved conduit: natural history and conduit performance under pressure. Eur J Cardiothorac Surg. 2006;29(3):397–405.
40. Tweddell JS, Pelech AN, Frommelt PC, et al. Factors affecting longevity of homograft valves used in right ventricular outflow tract reconstruction for congenital heart disease. Circulation. 2000;102 Suppl 3:130–5.
41. Bove T, Demanet H, Wauthy P, et al. Early results of valved bovine jugular vein conduit versus bicuspid homograft for right ventricular outflow tract reconstruction. Ann Thorac Surg. 2002;74:536–41.
42. Oosterhof T, van Straten A, Vliegen HW, et al. Preoperative thresholds for pulmonary valve replacement in patients with corrected tetralogy of Fallot using cardiovascular magnetic resonance. Circulation. 2007;116:545–51.
43. Khambadkone S, Bonhoeffer P. Nonsurgical pulmonary valve replacement: why, when, and how? Catheter Cardiovasc Interv. 2004;62:401–8.
44. Lurz P, Coats L, Khambadkone S, et al. Percutaneous pulmonary valve implantation: impact of evolving technology and learning curve on clinical outcome. Circulation. 2008;117(15):1964–72.
45. Schievano S, Coats L, Migliavacca F, et al. Variations in right ventricular outflow tract morphology following repair of congenital heart disease: implications for percutaneous pulmonary valve implantation. J Cardiovasc Magn Reson. 2007;9(4):687–95.
46. Nielsen E, Smerup M, Agger P, et al. Normal right ventricular three-dimensional architecture, as assessed with diffusion tensor magnetic resonance imaging, is preserved during experimentally induced right ventricular hypertrophy. Anat Rec (Hoboken). 2009;292(5):640–51.
47. Lev M, Bharati S, Meng CCL, Liberthson RR, Paul MH, Idriss F. A concept of double-outlet right ventricle. J Thorac Cardiovasc Surg. 1972;64:271–81.
48. Walters III HL, Mavroudis C, Tchervenkov CI, Jacobs JP, Lacour-Gayet F, Jacobs ML. Congenital heart surgery nomenclature and database project: double outlet right ventricle. Ann Thorac Surg. 2000;69(4 Suppl):S249–63.
49. Lacour-Gayet F, Maruszewski B, Mavroudis C, Jacobs JP, Elliott MJ. Presentation of the international nomenclature for congenital heart surgery. The long way from nomenclature to collection of validated data at the EACTS. Eur J Cardiothorac Surg. 2000;18:128–35.
50. Beekmana RP, Roest AA, Helbing WA, et al. Spin echo MRI in the evaluation of hearts with a double outlet right ventricle: usefulness and limitations. Magn Reson Imaging. 2000;18(3):245–53.
51. Mayo JR, Roberson D, Sommerhoff B, Higgins CB. MR imaging of double outlet right ventricle. J Comput Assist Tomogr. 1990;14(3):336–9.
52. Chen SJ, Lin MT, Liu KL, et al. Usefulness of 3D reconstructed computed tomography imaging for

double outlet right ventricle. J Formos Med Assoc. 2008;107(5):371–80.
53. Artrip JH, Sauer H, Campbell DN, et al. Biventricular repair in double outlet right ventricle: surgical results based on the STS-EACTS International Nomenclature classification. Eur J Cardiothorac Surg. 2006;29(4):545–50.
54. Barbero-Marcial M, Tanamati C, Atik E, Ebaid M. Intraventricular repair of double-outlet right ventricle with noncommitted ventricular septal defect: advantages of multiple patches. J Thorac Cardiovasc Surg. 1999;118:1056–67.
55. Hornung TS, Derrick GP, Deanfield JE, Redington AN. Transposition complexes in the adult: a changing perspective. Cardiol Clin. 2002;20:405–20.
56. Warnes CA. Transposition of the great arteries. Circulation. 2006;114:2699–709.
57. Paladini D, Volpe P, Sglavo G, et al. Transposition of the great arteries in the fetus: assessment of the spatial relationships of the arterial trunks by four-dimensional echocardiography. Ultrasound Obstet Gynecol. 2008;31(3):271–6.
58. Yasui H, Nakazawa M, Morishima M, Miyagawa-Tomita S, Momma K. Morphological observations on the pathogenetic process of transposition of the great arteries induced by retinoic acid in mice. Circulation. 1995;91(9):2478–86.
59. Mee RB. Severe right ventricular failure after Mustard or Senning operation: two-stage repair: pulmonary artery banding and switch. J Thorac Cardiovasc Surg. 1986;92(Pt 1):385–90.
60. Ebenroth ES, Hurwitz RA, Cordes TM. Late onset of pulmonary hypertension after successful Mustard surgery for d-transposition of the great arteries. Am J Cardiol. 2000;85:127–30.
61. Jatene AD, Fontes VF, Paulista PP, et al. Anatomic correction of transposition of the great vessels. J Thorac Cardiovasc Surg. 1976;72:364–70.
62. Blume E, Chung T, Hoffer FA, Geva T. Anatomically corrected malposition of the great arteries {S, D, L}. Circulation. 1998;97:1207.
63. Allwork SP, Bentall HH, Becker AE, et al. Congenitally corrected transposition of the great arteries: morphologic study of 32 cases. Am J Cardiol. 1976;38:910–23.
64. Hornung TS, Calder L. Congenitally corrected transposition of the great arteries. Heart. 2010;96:1154–61.
65. Prieto LR, Hordof AJ, Secic M, Rosenbaum MS, Gersony WM. Progressive tricuspid valve disease in patients with congenitally corrected transposition of the great arteries. Circulation. 1998;98:997–1005.
66. Van Praagh R. Truncus arteriosus: what is it really and how should it be classified? Eur J Cardiothorac Surg. 1987;1:65–70.
67. Calder L, Van Praagh R, Van Praagh S, et al. Truncus arteriosus communis: clinical, angiocardiographic, and pathologic findings in 100 patients. Am Heart J. 1976;92:23–38.
68. McGoon DC, Rastelli GC, Ongley PA. An operation for the correction of truncus arteriosus. JAMA. 1968;205:69–73.
69. Vida VL, Sanders SP, Bottio T, et al. Anomalous origin of one pulmonary artery from the ascending aorta. Cardiol Young. 2005;15:176–81.
70. Geva T, Powell AJ, Crawford EC, Chung T, Colan SD. Evaluation of regional differences in right ventricular systolic function by acoustic quantification echocardiography and cine magnetic resonance imaging. Circulation. 1998;98(4):339–45.
71. Nance Jr JW, Bastarrika G, Kang DK, et al. High-temporal resolution dual-energy computed tomography of the heart using a novel hybrid image reconstruction algorithm: initial experience. J Comput Assist Tomogr. 2011;35(1):119–25.
72. Geiger J, Markl M, Jung B, et al. 4D-MR flow analysis in patients after repair for tetralogy of Fallot. Eur Radiol. 2011;21(8):1651–7.
73. Johansson B, Babu-Narayan SV, Kilner PJ. The effects of breath-holding on pulmonary regurgitation measured by cardiovascular magnetic resonance velocity mapping. J Cardiovasc Magn Reson. 2009;11:1.
74. Sanchez-Quintana D, Anderson RH, Ho SY. Ventricular myoarchitecture in tetralogy of Fallot. Heart. 1996;76:280–6.
75. Anderson RH, Smerup M, Sanchez-Quintana D, Loukas M, Lunkenheimer PP. The three-dimensional arrangement of the myocytes in the ventricular walls. Clin Anat. 2009;22(1):64–76.
76. Lindqvist P, Henein M, Kazzam E. Right ventricular outflow-tract fractional shortening: an applicable measure of right ventricular systolic function. Eur J Echocardiogr. 2003;4(1):29–35.
77. Calcutteea A, Chung R, Lindqvist P, Hodson M, Henein MY. Differential right ventricular regional function and the effect of pulmonary hypertension: three-dimensional echo study. Heart. 2011;97(12):1004–11.
78. Denault AY, Chaput M, Couture P, Hébert Y, Haddad F, Tardif JC. Dynamic right ventricular outflow tract obstruction in cardiac surgery. J Thorac Cardiovasc Surg. 2006;132(1):43–9.
79. Geva T. Repaired tetralogy of Fallot: the roles of cardiovascular magnetic resonance in evaluating pathophysiology and for pulmonary valve replacement decision support. J Cardiovasc Magn Reson. 2011;13:9.
80. Bodhey NK, Beerbaum P, Sarikouch S, et al. Functional analysis of the components of the right ventricle in the setting of tetralogy of Fallot. Circ Cardiovasc Imaging. 2008;1(2):141–7.
81. d'Udekem Y, Ovaert C, Grandjean F, et al. Tetralogy of Fallot: transannular and right ventricular patching equally affect late functional status. Circulation. 2000;102(19 Suppl 3):III116–22.
82. Lytrivi ID, Ko HH, Srivastava S, et al. Regional differences in right ventricular systolic function as determined by cine magnetic resonance imaging after infundibulotomy. Am J Cardiol. 2004;94(7):970–3.
83. Wald RM, Redington AN, Pereira A, et al. Refining the assessment of pulmonary regurgitation in adults after tetralogy of Fallot repair: should we be

measuring regurgitant fraction or regurgitant volume? Eur Heart J. 2009;30(3):356–61.
84. Harris MA, Whitehead KK, Gillespie MJ, et al. Differential branch pulmonary artery regurgitant fraction is a function of differential pulmonary arterial anatomy and pulmonary vascular resistance. JACC Cardiovasc Imaging. 2011;4(5):506–13.
85. Babu-Narayan SV, Goktekin O, Moon JC, et al. Late gadolinium enhancement cardiovascular magnetic resonance of the systemic right ventricle in adults with previous atrial redirection surgery for transposition of the great arteries. Circulation. 2005;111:2091–8.
86. Davlouros PA, Niwa K, Webb G, Gatzoulis MA. The right ventricle in congenital heart disease. Heart. 2006;92(Suppl I):i27–38.
87. Pettersen E, Helle-Valle T, Edvardsen T, et al. Contraction pattern of the systemic right ventricle shift from longitudinal to circumferential shortening and absent global ventricular torsion. J Am Coll Cardiol. 2007;49:2450–6.
88. Graham Jr TP, Bernard YD, Mellen BG, et al. Long-term outcome in congenitally corrected transposition of the great arteries: a multi-institutional study. J Am Coll Cardiol. 2000;36:255–61.
89. Hauser M, Bengel FM, Hager A, et al. Impaired myocardial blood flow and coronary flow reserve of the anatomical right systemic ventricle in patients with congenitally corrected transposition of the great arteries. Heart. 2003;89:1231–5.
90. Wald RM, Haber I, Wald R, Valente AM, Powell AJ, Geva T. Effects of regional dysfunction and late gadolinium enhancement on global right ventricular function and exercise capacity in patients with repaired tetralogy of Fallot. Circulation. 2009;119(10):1370–7.
91. Tandri H, Saranathan M, Rodriguez ER, et al. Noninvasive detection of myocardial fibrosis in arrhythmogenic right ventricular cardiomyopathy using delayed-enhancement magnetic resonance imaging. J Am Coll Cardiol. 2005;45(1):98–103.
92. Boukens BJ, Christoffels VM, Coronel R, Moorman AF. Developmental basis for electrophysiological heterogeneity in the ventricular and outflow tract myocardium as a substrate for life-threatening ventricular arrhythmias. Circ Res. 2009;104(1):19–31.
93. Harrison DA, Harris L, Siu SC, et al. Sustained ventricular tachycardia in adult patients late after repair of tetralogy of Fallot. J Am Coll Cardiol. 1997;30(5):1368–73.
94. Globits S, Kreiner G, Frank H, et al. Significance of morphological abnormalities detected by MRI in patients undergoing successful ablation of right ventricular outflow tract tachycardia. Circulation. 1997;96(8):2633–40.
95. White RD, Trohman RG, Flamm SD, et al. Right ventricular arrhythmia in the absence of arrhythmogenic dysplasia: MR imaging of myocardial abnormalities. Radiology. 1998;207(3):743–51.
96. Miljoen H, State S, de Chillou C, et al. Electroanatomic mapping characteristics of ventricular tachycardia in patients with arrhythmogenic right ventricular cardiomyopathy/dysplasia. Europace. 2005;7(6):516–24.
97. Vaseghi M, Cesario DA, Mahajan A, et al. Catheter ablation of right ventricular outflow tract tachycardia: value of defining coronary anatomy. J Cardiovasc Electrophysiol. 2006;17(6):632–7.
98. Burke AP, Farb A, Tashko G, Virmani R. Arrhythmogenic right ventricular cardiomyopathy and fatty replacement of the right ventricular myocardium: are they different diseases? Circulation. 1998;97:1571–80.
99. Tansey DK, Aly Z, Sheppard MN. Fat in the right ventricle of the normal heart. Histopathology. 2005;46:98–104.
100. Raney AR, Saremi F, Kenchaiah S, et al. Multidetector computed tomography shows intramyocardial fat deposition. J Cardiovasc Comput Tomogr. 2008;2(3):152–63.
101. Tardif JC, Taylor K, Pandian NG, Schwartz S, Rastegar H. Right ventricular outflow tract and pulmonary artery obstruction by postoperative mediastinal hematoma: delineation by multiplane transesophageal echocardiography. J Am Soc Echocardiogr. 1994;7:400–4.
102. Stierle U, Sheikhzadeh A, Shakibi JG, Langbehn AF, Diederich KW. Right ventricular obstruction in various types of hypertrophic cardiomyopathy. Jpn Heart J. 1987;28:115–25.
103. Sirin BH, Kurdal AT, Iskesen I, Cerrahoglu M. Right ventricular outflow obstruction of the patient with biventricular non-compaction. Thorac Cardiovasc Surg. 2010;58(6):364–6.
104. Ross D. Pulmonary valve autotransplantation (the Ross operation). J Card Surg. 1988;3(Suppl):313–9.
105. Hraska V, Krajci M, Haun C, et al. Ross and Ross-Konno procedure in children and adolescents: mid-term results. Eur J Cardiothorac Surg. 2004;25(5):742–7.
106. Bjork VO, Olin CL, Bjarke BB, Thoren CA. Right atrial right ventricular anastomosis for correction of tricuspid atresia. J Thorac Cardiovasc Surg. 1979;77(3):452–8.